

THE DEEP ECLIPTIC SURVEY: A SEARCH FOR KUIPER BELT OBJECTS AND CENTAURS. I. DESCRIPTION OF METHODS AND INITIAL RESULTS

R. L. MILLIS,¹ M. W. BUIE,¹ AND L. H. WASSERMAN¹
Lowell Observatory, 1400 West Mars Hill Road, Flagstaff, AZ 86001

J. L. ELLIOT^{1,2} AND S. D. KERN
Department of Earth, Atmospheric, and Planetary Sciences, Massachusetts Institute of Technology,
77 Massachusetts Avenue, Cambridge, MA 02139

AND

R. M. WAGNER¹
Large Binocular Telescope Observatory, University of Arizona, Tucson, AZ 85721
Received 2001 July 19; accepted 2001 December 28

ABSTRACT

We report here initial results of the Deep Ecliptic Survey, an ongoing new search for Kuiper belt objects (KBOs) and Centaurs using the 8K × 8K Mosaic CCD array on the 4 m Mayall Telescope at Kitt Peak National Observatory. Within the interval covered in this paper, useful observations were obtained during seven nights in 1998 October and November, 1999 April, and 2000 February. We used a novel technique to efficiently find and determine positions of moving objects. Sixty-nine KBOs and Centaurs with apparent magnitudes between 20.6 and approximately the 24th magnitude were discovered. Nine or 10 of the newly discovered KBOs appear to be in the 3 : 2 mean motion resonance with Neptune, and four appear to be scattered-disk objects. Three objects were found that may be in the 4 : 3 resonance. Sixty-two of the objects reported here have been observed on at least one additional night and have received designations. Our own follow-up astrometry was done primarily with the WIYN 3.5 m telescope in queue-scheduled mode and with the Steward Observatory 90 inch (2.3 m) telescope. Others, using a variety of telescopes, recovered a significant number of our objects. Although not a primary objective of the survey, positions of all main-belt asteroids, Trojan asteroids, and nearby fast-moving asteroids seen in our data also have been determined, and most have been reported to the Minor Planet Center. Through simulations and analysis of the existing KBO database, we have investigated the uncertainty to be expected in various KBO orbital parameters as a function of the extent of the astrometric coverage. The results indicate that the heliocentric distance of an object and the inclination of its orbit can be narrowly constrained with observations from a single apparition. Accurate determination of semimajor axis and eccentricity, on the other hand, requires astrometric data extending over additional apparitions. Based on the observed distribution of orbital inclinations in our sample, we have estimated the true distribution of orbital inclinations in the Kuiper belt and find it to be similar to that of the short-period comets. This result is consistent with the commonly held belief that the Kuiper belt is the source region of the short-period comets.

Key words: astrometry — comets: general — Kuiper belt — methods: observational — planets and satellites: general — solar system: general — surveys

1. INTRODUCTION

The discovery of the Kuiper belt (Jewitt & Luu 1993) and the subsequent exploration of this region by a number of investigators have been among the most exciting developments in modern planetary astronomy. An enormous region of the solar system, previously thought by some to be essentially devoid of material, is now known to be populated by vast numbers of small and, perhaps, some not-so-small bodies orbiting the sun beyond Neptune. While only a minuscule fraction of the total population of Kuiper belt objects (KBOs) has been discovered, those KBOs we do know about display remarkable diversity in their physical characteristics (Barucci et al. 2000; Brown 2000; Davies et

al. 2000; Jewitt & Luu 1998; Luu & Jewitt 1996; Tegler & Romanishin 1997) and have orbital properties that undoubtedly hold valuable clues to the dynamical evolution of the outer solar system (Holman & Wisdom 1993; Levison & Duncan 1997; Malhotra 1995).

Early searches for KBOs apparently were motivated primarily by the theoretical work of several investigators, including Fernández (1980) and Duncan, Quinn, & Tremaine (1988). These authors showed that the observed population of short-period comets could not have originated from the Oort cloud but required instead a source region more closely constrained to the plane of the ecliptic. Luu & Jewitt (1988), Kowal (1989), Levison & Duncan (1990), and Cochran, Cochran, & Torbett (1991), conducted searches using telescopes of modest aperture and either photographic plates or small-format CCDs. These searches were uniformly unsuccessful, primarily because their limiting magnitudes were too bright, their sky coverage too small, or both. Tyson et al. (1992) used a 1k × 1k CCD on the 4 m Blanco Telescope at Cerro Tololo Inter-Ameri-

¹ Visiting Astronomer, Kitt Peak National Observatory, National Optical Astronomy Observatory, which is operated by the Association of Universities for Research in Astronomy, Inc., under cooperative agreement with the National Science Foundation.

² Also Department of Physics, Massachusetts Institute of Technology.

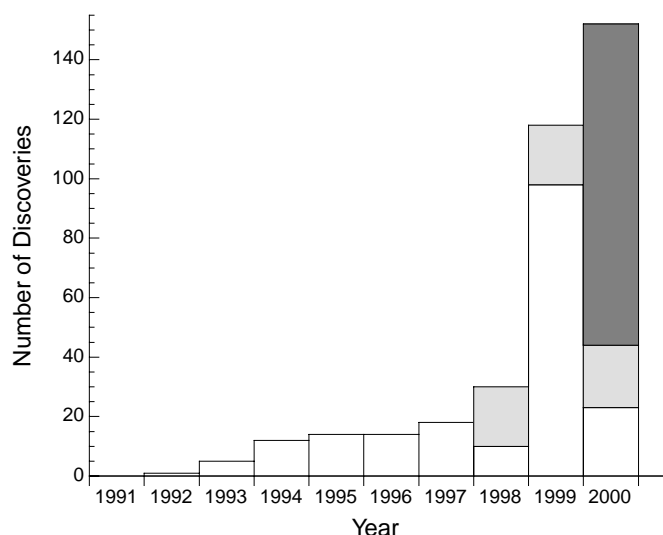


FIG. 1.—Number of KBOs that have received designations from the Minor Planet Center vs. year. The light gray segments indicate the observations discussed in this paper. The dark portion of the rightmost bar indicates KBOs discovered in 2000 after the cutoff date for data included in this paper.

can Observatory (CTIO) in a very limited but equally unsuccessful search. Undeterred by the initial lack of success, Jewitt & Luu continued searching with remarkable perseverance, sometimes with a $1\text{K} \times 1\text{K}$ CCD and other times with a $2\text{K} \times 2\text{K}$ CCD, on the University of Hawaii 2.2 m telescope. After devoting 4 years to this extended search and having covered 0.7 deg^2 of sky, they were rewarded with the first discovery of a KBO, 1992 QB₁ (Jewitt & Luu 1993). Spurred on by the discovery of 1992 QB₁, Jewitt & Luu, along with other investigators, intensified their search efforts. As is seen in Figure 1, by 1997 the annual rate of discovery had grown to a high of 18. The following year, the Mosaic camera became operational at Kitt Peak National Observatory (Muller et al. 1998). When used at the prime focus of the 4 m Mayall Telescope, it is possible with this large-format camera to image $0.6^\circ \times 0.6^\circ$ on the sky to approximately $R = 24$ mag (under good seeing conditions) with a single 5 minute exposure. Consequently, in two exposures with the Mosaic camera, one could image as much of the sky as was covered by Jewitt & Luu in the first 4 years of their search. In this paper, we describe the methods and initial results of a search for KBOs and Centaurs that we have begun at Kitt Peak National Observatory with Mosaic.

2. INSTRUMENTATION AND OBSERVATIONAL APPROACH

2.1. Camera

The Mosaic camera consists of eight edge-abutted 2048×4096 thinned, antireflection-coated SITe CCDs with $15 \mu\text{m}$ pixels (Muller et al. 1998). (Our first run in 1998 March occurred while engineering-grade, unthinned CCDs were in the camera, but because of poor weather only a very small amount of test data were obtained during that run.) Each pixel corresponds to $0.26'' \times 0.26''$ on the sky. We used the atmospheric dispersion corrector (ADC) for all observations. While the image quality was generally uniform across

the field, we did note significant and variable geometric distortions, perhaps introduced by the ADC, that required special consideration in order to derive accurate positions of the objects discovered.

2.2. Search Strategy

Different investigators have employed a variety of search strategies in the exploration of the Kuiper belt. Some (e.g., Jewitt, Luu, & Trujillo 1998) have sought to maximize sky coverage at the expense of accepting a brighter limiting magnitude. Luu & Jewitt (1998), Gladman et al. (1998), Chiang & Brown (1999), and Allen, Bernstein, & Malhotra (2001), on the other hand, have conducted pencil-beam surveys in which a comparatively small area of the sky is searched to the faintest possible limiting magnitude. Both approaches have their merits and, to a degree, address overlapping objectives. For example, both are important to learning the cumulative sky density of KBOs as a function of apparent magnitude (the so-called luminosity function) and to understanding the size distribution and total mass of objects in the Kuiper belt. An important difference between the two approaches, however, is that objects found by the “traditional” search strategy are usually sufficiently bright that they can be recovered and their orbits eventually accurately determined, while objects discovered in the pencil-beam surveys are often so faint that follow-up astrometry is not practical. Furthermore, only through wide surveys will a significant sample of KBOs bright enough for diagnostic physical observations be found.

For the search discussed in this paper, we have adopted an essentially traditional strategy, but we have worked to hone that strategy with the aim of maximizing the rate of KBO discovery. Time on 4 m telescopes with large CCD arrays is extremely valuable. Consequently, we have developed procedures that require modest additional effort in preparing for an observing run and a substantially more astronomer-intensive approach to analyzing the resulting data in order to make the most effective use of the time at the telescope. That our approach produces a high rate of discovery is demonstrated by the results discussed in this paper. We believe it will contribute importantly to a much better defined picture of the dimensions of the Kuiper belt, the distribution of objects within the belt, and ultimately to a better understanding of the processes that have been important beyond Neptune over the age of the solar system.

Our survey is still very much a work in progress. As indicated below, our techniques have evolved over time, and we expect they will continue to be refined.

2.3. Choice of Exposure Time

When taking conventional stare-mode exposures, one usually chooses an exposure time in order to reach a certain limiting magnitude. With this mode, in searches for moving objects, a point of rapidly diminishing returns is reached. In particular, one gains nothing by exposing longer than it takes an object to move a significant fraction of the seeing disk. For objects near opposition in the main Kuiper belt, Earth’s reflex motion is roughly $2''\text{--}3'' \text{ hr}^{-1}$. If the seeing is $1''$, one would not want to expose longer than about 10 minutes. On the other hand, if one’s objective is to maximize the discovery rate, shorter exposures with the resulting greater sky coverage may be preferred. Another factor to consider is the Mosaic readout time, which at the time of

our observations ranged from about 1 to nearly 2 1/2 minutes. We chose an exposure time of 300 s because such an exposure was long enough to detect KBOs throughout the classical Kuiper belt, while still ensuring that we spent most of the night collecting photons instead of reading out the CCD, as would have been the case with much shorter exposures.

2.4. *Expected Limiting Magnitude*

The Mosaic camera has a standard set of broadband filters, along with a “white” filter made of BK7 glass that transmits the entire optical spectrum. (The purpose of this filter is to permit full-spectrum imaging while maintaining the focus at a setting close to that of the other filters.) The exposure calculator on the KPNO Web site indicated that one could achieve a signal-to-noise ratio of 10 at a limiting R magnitude of 23.9 with a 300 s exposure assuming 1"1 seeing, an air mass of 1.2, and new Moon. Since the exposure calculator did not include an option for the white filter, we carried out our own calculation for a faint object of solar color and found that we should expect to achieve a signal-to-noise ratio with the white filter that was more than twice that of the R filter (despite the bright night-sky OH emission features in the near-IR). Assuming a limiting magnitude of 23.9 in R , we calculated an expected limiting magnitude of 24.6 in the white filter. As will be seen later in the paper, this calculation appears to have been overly optimistic, but it nevertheless guided our choice of the white filter for our observations in 1998 and 1999. In 2000, a Sloan r' filter became available for use with the Mosaic camera, and we adopted it for our observations beginning in February of that year. This filter excludes most of the OH night-sky emission, while still maintaining a broad bandpass. The r' filter is more efficient than both the R and the white filters, though a VR filter similar to that used by Jewitt, Luu, & Chen (1996) would have been still better.

2.5. *Selection of Search Fields*

Selection of fields to be searched in this program was designed to maximize the rate of KBO discovery. Field centers for any given observing run were confined to within $\pm 6.5^\circ$ of the ecliptic and spanned a swath along the ecliptic initially of $\pm 45^\circ$ from the opposition point. Later the search window was narrowed to $\pm 30^\circ$ in ecliptic longitude. An edge-to-edge grid of fields was selected filling this zone, but fields containing stars brighter than 9.5 mag (as indicated in the PPM catalog) were rejected. Bright stars produce significant blooming on the image that substantially reduces the area of the chip where detection of faint objects is possible. Likewise, fields having fewer than 35 astrometric standards (from the USNO-A2.0 catalog) per CCD in the Mosaic array were also excluded. The geometric distortions across the Mosaic field, in our experience, require this number of astrometric standards to derive accurate coordinates for the KBOs discovered. This is particularly true for objects falling on the CCDs at the corners of the array. A star chart showing a typical distribution of fields meeting our requirements is shown in Figure 2. Without exception, far more fields meeting our constraints were available than could be observed in a given two-night run. Selection of fields to actually be observed was done at the telescope in response to the particular circumstances of the night. All things being equal, we attempted to observe as many fields as possible

near the opposition point, but, in order to fully use the night and restrict our observations to less than 2 air masses, it was necessary to include fields up to 2–3 hr east and west of opposition.

2.6. *Sequence of Observations*

For each field chosen for observation, in 1998 and 1999 we, like most earlier observers using a non-pencil-beam strategy (e.g., Irwin, Tremaine, & Żytkow 1995; Jewitt et al. 1998; Rousselot, Lombard, & Moreels 1999; Sheppard et al. 2000), initially took three exposures separated at intervals of approximately 2 hr. Sometimes circumstances on a given night, such as the arrival of clouds, required departure from this scheme. In principle, two exposures are adequate for finding moving objects, but a third exposure can sometimes provide useful confirmation. However, over time we became convinced that only rarely was this confirmation essential to the positive discovery of a KBO, and beginning in 2000 we began taking only two exposures per search field. In either case, on each night 5 minute exposures were taken relentlessly throughout the night, resetting the telescope as rapidly as possible during readout of the CCDs.

On-chip binning was not initially available with the thinned CCDs used to acquire the data discussed in this paper. Consequently, in late 1998 and throughout 1999, slightly more than 2 minutes had to be devoted to readout of the CCDs following each exposure. By early 2000, on-chip binning was implemented on the Mosaic camera reducing readout time to about 70 s. We used that feature during the 2000 February run.

Ordinarily the telescope can be set on the next field during readout of the CCD, giving an overall cycle time per exposure of roughly 6–7 minutes, depending on whether binning is being used. Hence, during 1998 and 1999 in a 10 hr clear night we could, in principle, cover 10 deg^2 visiting each field three times. In actual practice the best we achieved was 11.5 deg^2 on 1998 November 19, when our observations spanned a full 10.25 hr. However, on that night several fields were visited only twice, and one was visited only once. With the shorter readout time available in 2000 and the reduction to two exposures per search field, we were able to increase our sky coverage to 15.8 deg^2 during 10.5 hr on our best night, February 5.

2.7. *Observations*

The nights allocated for this program are listed in Table 1. The 1998 November, 1999 April, and 2000 February runs offered the best conditions, but useful observations were also obtained during the 1998 October run. The 1998 March run was almost a total loss, and the one in 1999 March suffered both from poor seeing and clouds. Of the 13 nights allocated to the program through 2000 February, seeing and transparency were good enough to carry out useful observations for this program on seven nights, although some data were taken on all but one of the other nights.

2.8. *Limiting Magnitude Achieved*

We estimated the detection limit for each frame by calculating the total number of counts within a Gaussian point-spread function with a FWHM equal to the mean seeing of the image and a height equal to twice the standard deviation of the sky signal (2σ). The limiting source so defined was then treated the same as any object measured in the field

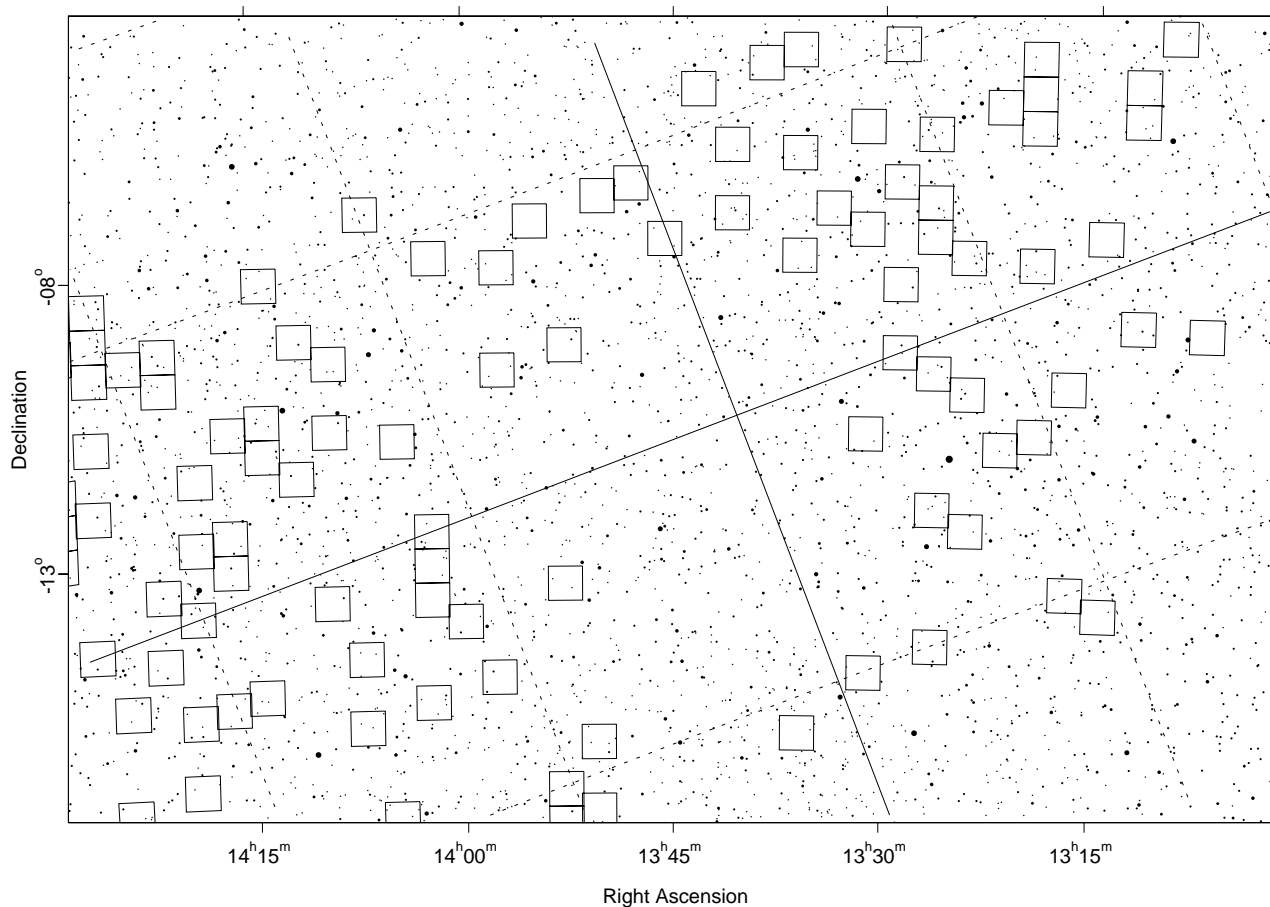


FIG. 2.—Sample map of search fields meeting the criteria of the Deep Ecliptic Survey. Each square is the size of a single Mosaic exposure. Declination is plotted along the ordinate, right ascension along the abscissa. The solid line running from lower left to upper right indicates the ecliptic. The intersection of the ecliptic with the other solid line indicates the location of the opposition point for the date of the chart. The dashed lines are spaced at intervals of 5° .

using the same aperture and photometric zero point. Our magnitude scale was set by an average of the red magnitudes of all USNO-A2.0 catalog stars on each frame. We find that based on our observations obtained on 1999 April 17–18 that our 2σ detection limit with the white filter is 23.9 ± 0.1 mag for a 300 s exposure, $1''.2$ seeing FWHM, and standard deviation of the sky per pixel of 25 DN. The gain of the Mosaic amplifier was $3 e^- \text{ADU}^{-1}$. This 2σ detection limit is statistically meaningful for determination of false-positive detections. However, experience has shown that real 2σ objects are readily detected at the 50% efficiency level. In observations aimed at recovery of previously discovered objects, where the approximate position of the moving object is known, images fainter than 2σ still yield good astrometry, but photometry quickly becomes very uncertain.

3. DATA PROCESSING AND DETECTION TECHNIQUE

As mentioned above, our techniques for processing the vast amount of data collected were subject to considerable experimentation and evolved substantially over the interval discussed in this paper. Bias correction was done in the usual fashion, while both dome flats and sky flats were tried. In agreement with other Mosaic users, we found that twilight sky and dome flats were not adequate. Instead, a high-quality flat-field frame was constructed for each night by

median filtering 10–15 well-exposed bias-subtracted search frames of different fields obtained at relatively low air mass. In 1998 and 1999 we initially worked with the unbinned $8K \times 8K$ images but ultimately migrated to 2×2 binning of the data prior to processing or analysis. Experiments showed that this approach did not decrease the KBO detection rate, and it greatly reduced the data processing and storage requirements. By the time of the 1999 April run our techniques had advanced to the point that binning, bias correction, and flattening of the data were accomplished “on the fly” at the telescope as data were being collected.

Most other investigators who have conducted large-scale KBO searches using the traditional approach have adopted a largely automatic process for detecting moving objects. Excellent examples of this approach have been described by Levison & Duncan (1990), Trujillo & Jewitt (1998), and Rousselot et al. (1999). In this approach three or more exposures spaced in time are taken of each search field on a given night. The digital images are then evaluated by sophisticated software to identify slowly moving objects that are then confirmed by direct inspection with classical blinking. This type of approach has the advantage that it is less labor intensive and may produce results that are more immune to subjective effects. However, automated methods of detection do produce a nonnegligible number of false detections that must be eliminated by direct inspection of the images,

TABLE 1
LOG OF OBSERVATIONS

Local Date Scheduled	Start (UT)	End (UT)	Fields	Coverage (deg ²)	KBOs Found	Designated Objects	Comments
1998 Mar 24/25 ...	0601	0752	Closed because of high wind
1998 Mar 25/26 ...	0250	0350	Closed because of high wind
1998 Mar 26/27	Night lost entirely to weather
1998 Oct 20/21	0401	0634	5	1.8	Intermittent clouds throughout, closed because of weather
1998 Oct 21/22	0248	1212	16	5.8	3	1998 UR ₄₃ , 1998 US ₄₃ , 1998 UU ₄₃	Intermittent clouds throughout, closed because of weather
1998 Nov 17/18 ...	0215	1233	26	9.4	13	1998 WG ₂₄ , 1998 WV ₂₄ , 1998 WX ₃₁ , 1998 WY ₃₁ , 1998 WW ₃₁ , 1998 WU ₃₁ , 1998 WT ₃₁ , 1998 WS ₃₁ , 1998 WA ₃₁ , 1998 WZ ₂₄ , 1998 WY ₂₄ , 1998 WX ₂₄ , 1998 WW ₂₄	Closed from 0630 until 0900 UT because of high wind
1998 Nov 18/19 ...	0121	1250	31	11.2	4	1998 WH ₂₄ , 1998 WZ ₃₁ , 1998 WV ₃₁ , 1998 WA ₂₅	Scattered cirrus at dusk
1999 Mar 15/16 ...	0230	1001	19	6.8	Closed because of clouds
1999 Mar 16/17 ...	0856	1215	0	Clouds early, poor night
1999 Apr 16/17....	0256	1127	20	7.2	8	1999 HX ₁₁ , 1999 HY ₁₁ , 1999 HZ ₁₁ , 1999 HA ₁₂ , 1999 HR ₁₁ , 1999 HS ₁₁ , 1999 HT ₁₁ , 1999 HD ₁₂	Much cirrus but usable
1999 Apr 17/18....	0305	1130	20	7.2	11	1999 HB ₁₂ , 1999 HC ₁₂ , 1999 HU ₁₁ , 1999 HV ₁₁ , 1999 HW ₁₁ , 1999 HG ₁₂ , 1999 HH ₁₂ , 1999 HJ ₁₂	Cirrus at sunset, clear at dawn
2000 Feb 4/5.....	0140	1250	47	16.9	15	2000 CL ₁₀₄ , 2000 CM ₁₀₄ , 2000 CN ₁₀₄ , 2000 CE ₁₀₅ , 2000 CF ₁₀₅ , 2000 CG ₁₀₅ , 2000 CH ₁₀₅ , 2000 CJ ₁₀₅ , 2000 CO ₁₀₅ , 2000 CP ₁₀₅ , 2000 CQ ₁₀₅ , 2000 CY ₁₀₅ , 2000 CM ₁₁₄ , 2000 CN ₁₁₄ , 2000 CO ₁₁₄	Excellent seeing most of the night
2000 Feb 5/6.....	0627	1321	29	10.4	15	2000 CO ₁₀₄ , 2000 CP ₁₀₄ , 2000 CQ ₁₀₄ , 2000 CK ₁₀₅ , 2000 CL ₁₀₅ , 2000 CM ₁₀₅ , 2000 CN ₁₀₅ , 2000 CR ₁₀₅ , 2000 CS ₁₀₅ , 2000 CP ₁₁₄ , 2000 CQ ₁₁₄	Cloudy first half of night

and more seriously, they may fail to detect real objects when the body is too close to a star or galaxy on one or more of the exposures.

In the initial scrutiny of our early data we used solely an automatic detection algorithm. However, we were discouraged by the high false-positive rate and as a result augmented the automated approach with a novel direct inspection technique that had been developed earlier for recovery of asteroids. With this approach two images of a given field are displayed on a 24 bit color monitor, with the first of the two exposures projected in the red plane of the display and the second projected in the blue and green (cyan) planes. The two frames are registered (to the nearest pixel) so that stars and other fixed sources are superposed on the display and hence appear essentially white. Objects that are in different relative positions on the two frames, however, will be displaced on the computer display and will appear as red-cyan pairs of images (see Fig. 3). The colors quickly catch the eye, and the reality of the moving object can easily be confirmed by the classical blinking mode provided by the software. The software also permits the X - Y positions of the moving objects to be recorded by placing the cursor over each image and clicking. The positions are determined either by an automatic centroiding routine or, in the case of blended images or cosmic-ray contamination, by visual estimation of the position. In instances when a third exposure is available, the reality of the object can be

unequivocally confirmed by carrying out the color comparison again, this time comparing the first and third exposures of the field being searched. The position of the object in the third image is then marked in the same fashion.

We found visual inspection of our data to be an efficient means of detecting moving objects. Scanning a given field and marking all moving objects seen—including main-belt, Trojan, and fast-moving asteroids—typically took only a few minutes. (Indeed, the search often began in the telescope control room as soon as the first pair of exposures of a given field had been completed and flattened. A number of the KBOs reported here were discovered at the telescope as observations were in progress.) To avoid, to the extent possible, overlooking moving objects, each field was first searched using the automated software and then independently scanned visually by at least two individuals on our team.

Extensive tests were undertaken of the effectiveness of our detection scheme as a function of moving-object magnitude. In these tests pairs of actual Mosaic exposures of search fields from the Mayall Telescope were “salted” with artificial KBO images having the same point-spread function as stellar images on those frames. The simulated KBOs were randomly placed on the frames, and their directions and rates of motion were also randomized within limits appropriate for objects in the Kuiper belt. Likewise, the magnitudes of the artificial images were adjusted to span a range

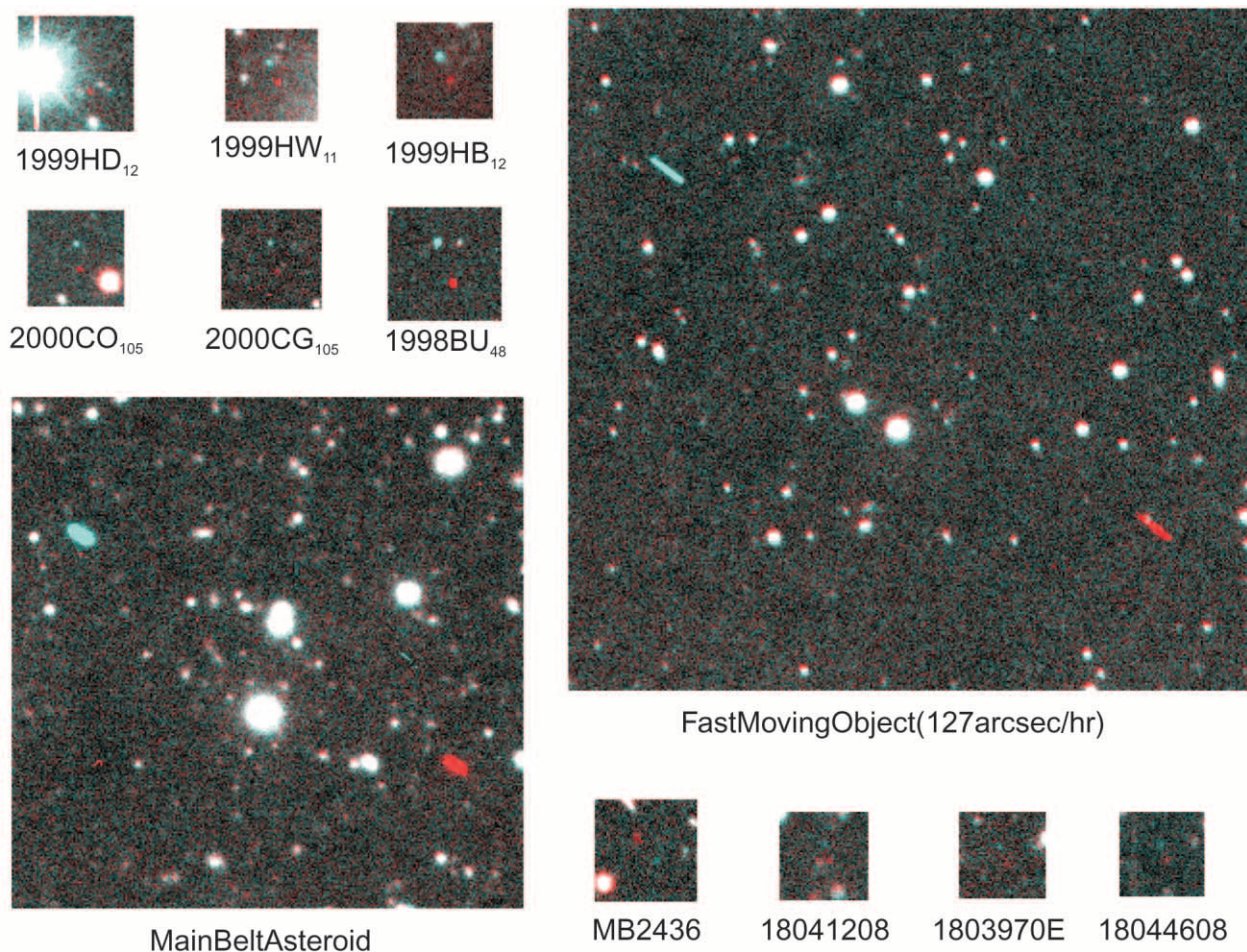


FIG. 3.—Sample images of moving objects as they appear with the detection technique described in this paper. Stationary objects appear white in the color images, while moving objects are seen as red-cyan pairs. The two larger squares illustrate the appearance of relatively rapidly moving objects such as main-belt asteroids. The smaller squares show the appearance of 10 objects or possible objects moving at rates appropriate to the Kuiper belt. Objects such as 1999 HB₁₂ and 1999 BU₄₈ are relatively bright and easy to find. Objects such as 2000 CG₁₀₅ are fainter but still readily detectable. 1803970E and 18044608 are near the limit at which we can detect moving objects with certainty, while 18041208 is perhaps at or below that limit. Observant readers will have noted that MB 2436, while quite bright, is moving in the opposite direction. This object is one of several enigmatic objects detected in the survey that we do not as yet have the resources to follow up.

from 2 mag above the limiting magnitude to 2 mag below that value. These salted frames were then searched in the same fashion as the “real” data using both software and the direct inspection method. The fraction of salted objects found during the examination of these frames is shown as a function of magnitude in Figure 4. The limiting magnitude of these exposures as defined earlier is indicated by the “relative magnitude = 0” point on the abscissa. Note that the technique was highly effective nearly to the limiting magnitude. Moreover, the outcome seemed largely independent of who was doing the visual searching (one of the participants in the test had little experience with the method).

Although our automatic detection algorithm has subsequently been greatly refined, we have concluded that the extra effort of direct inspection is worthwhile for our survey given our goal of maximizing the rate of KBO discovery. With the automatic approach alone, one has effectively no chance of finding anything missed by the software, and, more importantly, it is only through adoption of the direct inspection approach that we are able to search effectively with just two exposures per field. With only two exposures per field, the false-positive rate with automatic detection techniques is very high.

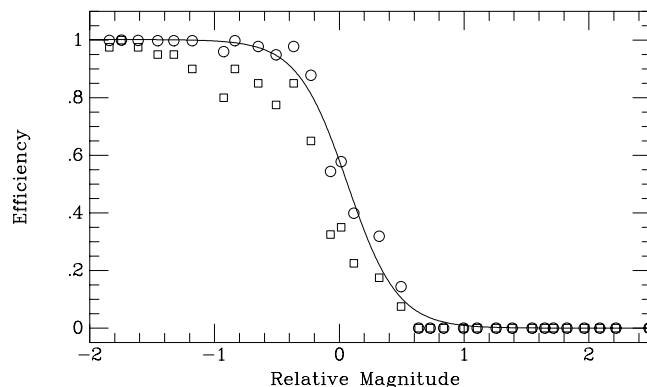


FIG. 4.—Efficiency of detection vs. relative apparent magnitude (limiting magnitude = 0). Squares represent the case in which the observations were scrutinized by the automatic detection software plus a single visual inspection of the images. Open circles indicate the results when two individuals independently scanned the images. The solid curve has been fitted to the open circles.

4. ASTROMETRY AND PHOTOMETRY

4.1. *Description of Astrometric Method*

Once a moving object had been identified and its location measured, the positions next were converted from sky-plane X - Y coordinates to astrometric right ascension and declination. To establish the astrometric transformation, each CCD within the $8K \times 8K$ mosaic was treated separately. Not only are the field distortions on each quite different, but the relative distortions change with zenith distance, thus preventing a global solution that would require only a zero-point shift or other low-order correction. As a consequence, the field covered by each CCD must include an adequate number of astrometric reference stars to permit a good solution. The Mosaic images have quite strong distortions and a cubic astrometric solution (this includes 10 terms in each axis: constant, x , y , r , x^2 , y^2 , x^3 , y^3 , xy^2 , x^2y) is needed. As mentioned earlier, to ensure a well-constrained fit, we pre-selected our fields so that each CCD contained at least 35 reference stars from the USNO-A2.0 catalog. The typical residual in the astrometric solution was $0''.25$ – $0''.5$ per reference star. The overall quality of the astrometric solution was completely dominated by catalog and proper-motion errors.

4.2. *Photometric Calibration of the Frames*

An instrumental magnitude for all objects on each CCD frame was determined with synthetic aperture photometry as described by Buie & Bus (1992). This approach provides quite good differential instrumental magnitudes for all objects in the frame, within, of course, the limits imposed by signal-to-noise considerations. We then used the red magnitudes of the astrometric reference stars from the USNO-A2.0 catalog to derive an average zero-point correction between our instrumental magnitudes and the catalog's red magnitudes. The photometric quality of the USNO catalog is known to suffer nonnegligible zonal errors. B. Skiff (2001, private communication) has compared the A2.0 magnitudes against numerous deep photometric sequences in the literature. For regions north of -17° declination, which includes all of the fields discussed in this paper, he found in the case of stars fainter than 16th magnitude the A2.0 red magnitudes ordinarily to be within ± 0.3 mag of the Cousins R magnitudes with occasional discrepancies as large as ± 0.5 mag.

Additional uncertainty springs from the fact that the filters used in our search were chosen to maximize the signal-to-noise ratio and not to match any standard photometric system. We have investigated these effects using Mosaic exposures of the standard area in Hercules discussed by Majewski et al. (1994). These authors have determined accurate $UBVRI$ magnitudes and color indexes for 13 stars in this area between $R = 16.4$ and $R = 21.4$ mag with $V-R$ ranging from 0.30–0.99 mag. We observed this field through the “white” and Sloan r' filters on a number of occasions. Magnitudes were derived for the standard stars by the same approach as for the KBOs—namely, the Buie & Bus algorithm was used to derive instrumental magnitudes and a zero-point correction was applied based on USNO A2.0 stars in the field. In the case of the r' filter, the difference between the magnitudes we derived and the standard R magnitudes quoted by Majewski et al. was less than ± 0.08 mag across the entire magnitude and color range of the 13

standards. In the case of observations of the standard field through the white filter, the magnitudes we derived were in almost all instances within ± 0.3 mag of the Majewski et al. values. Furthermore, over the color range of $V-R$ from $+0.4$ to $+0.8$ typical of KBOs, we saw no evidence of a significant color dependence in the derived magnitudes except, perhaps, at the very red end of the sequence.

In summary, we are convinced that the magnitudes quoted in Table 3 are ordinarily accurate to a few tenths of a magnitude. These values are therefore sufficiently accurate for their intended purpose of guiding future astrometric or physical measurements. Buie has undertaken a program with the robotic 31 inch (0.8 m) telescope at Lowell Observatory to establish accurate secondary photometric standards within each of our search fields. When this has been accomplished, we will be able to derive significantly more accurate photometry from our existing data and we will be able to consider issues such as the KBO luminosity function. In the meantime, we note that none of the results of this paper are dependent in any way on the magnitudes quoted in Table 2.

5. RECOVERY OF OBJECTS DISCOVERED AND ORBIT DETERMINATION

While a survey that simply discovers KBOs can provide statistically useful information, a much greater scientific return is realized if appropriately spaced astrometric measurements are subsequently made for each new object. At least one such follow-up measurement is required to secure an “official” designation from the Minor Planet Center (MPC), but more importantly, additional astrometry is essential over an extended period if the orbits are to be sufficiently refined to allow dynamical studies of the belt and assured recovery of the objects in future apparitions. Moreover, without accurate ephemerides, physical studies with large telescopes of newly discovered KBOs are either not possible or are very inefficient.

5.1. *Recovery Strategy*

Because KBOs move so slowly across the sky, recovery observations, unless delayed by months, do not require the wide field of view of the Mosaic camera. Accordingly, when possible, we attempted recovery of the objects discovered in this search initially with the NFIM $2K \times 2K$ CCD camera on the WIYN 3.5 m telescope and subsequently with the $4K \times 4K$ MiniMosaic camera that became available on that telescope in 2000. These observations were obtained by NOAO staff members during queue-scheduled time on the telescope. Our program was well suited to this operational mode because the observations were not particularly time-critical, could be taken any time during the night (provided the object was not at too high an air mass), and required only two or three brief exposures per object. Of the 69 KBOs and Centaurs discovered in this program, 28 were recovered during queue-mode observations at the WIYN Telescope, 21 objects (including one independently recovered at the WIYN Telescope) were recovered by M. Holman and colleagues using the 2.6 m Nordic Optical Telescope at La Palma, one was recovered with the Isaac Newton Telescope—also on La Palma—by E. Fletcher and A. Fitzsimmons. Of the remaining objects, four were recovered at the Mayall Telescope in the normal course of our observing

TABLE 2
LOG OF DISCOVERIES

Designation (1)	Discovery (2)	R.A. (3)	Decl. (4)	App. Mag. (5)	Recovery Telescope (6)	MPC No. (7)
19521	1998 Nov 19.41122	03 35 39.49	+20 47 23.4	20.56	Perkins	1998-X08
1998 UR ₄₃	1998 Oct 22.35531	02 20 42.94	+11 07 23.2	22.6	Mayall	1998-X05
1998 US ₄₃	1998 Oct 22.40628	03 08 48.43	+16 39 15.3	22.8	Mayall	1998-X06
1998 UU ₄₃	1998 Oct 22.35003	02 17 47.55	+16 18 22.5	22.5	INT	1999-B23
1998 WG ₂₄	1998 Nov 18.43221	05 00 31.48	+22 14 15.4	22.1	Mayall	1998-X07
1998 WV ₂₄	1998 Nov 18.12480	02 45 33.31	+14 56 32.1	22.6	WIYN	1998-X12
1998 WW ₂₄	1998 Nov 18.14057	03 05 15.15	+18 38 37.6	22.3	WIYN	1998-X13
1998 WX ₂₄	1998 Nov 18.38490	03 25 15.39	+18 34 38.3	22.5	WIYN	1998-X14
1998 WY ₂₄	1998 Nov 18.43762	04 59 35.44	+21 49 05.4	22.6	WIYN	1998-X15
1998 WZ ₂₄	1998 Nov 18.44295	05 03 14.47	+22 28 13.0	22.5	WIYN	1998-X16
1998 WA ₂₅	1998 Nov 19.22553	03 09 05.16	+16 33 14.2	22.8	WIYN	1998-X17
1998 WA ₃₁	1998 Nov 18.08751	02 14 16.22	+16 26 29.7	22.8	Mayall	1998-X38
1998 WS ₃₁	1998 Nov 18.09812	02 17 37.85	+16 33 43.0	22.5	NOT	1999-A15
1998 WT ₃₁	1998 Nov 18.11955	02 43 38.73	+17 19 52.0	22.6	NOT	1999-A16
1998 WU ₃₁	1998 Nov 18.14057	03 07 05.71	+18 27 14.7	23.0	NOT	1999-A17
1998 WV ₃₁	1998 Nov 19.09014	02 29 45.19	+12 45 25.3	22.3	NOT	1999-A18
1998 WW ₃₁	1998 Nov 18.21509	03 21 32.64	+18 59 07.3	22.6	WIYN/NOT	1999-B24
1998 WX ₃₁	1998 Nov 18.41641	04 24 39.16	+23 11 38.2	22.1	WIYN	1999-B25
1998 WY ₃₁	1998 Nov 18.42696	04 49 19.14	+22 47 19.1	23.1	WIYN	1999-B26
1998 WZ ₃₁	1998 Nov 19.41122	03 35 42.14	+20 59 22.1	22.7	WIYN	1999-B27
1999 HR ₁₁	1999 Apr 17.16538	12 41 52.69	-00 59 36.5	22.9	NOT	1999-K12
1999 HS ₁₁	1999 Apr 17.20248	13 34 18.65	-07 00 48.9	22.2	NOT	1999-K12
1999 HT ₁₁	1999 Apr 17.24637	13 42 01.28	-05 39 49.6	23.1	NOT	1999-K12
1999 HU ₁₁	1999 Apr 18.20550	13 29 32.70	-09 11 28.1	22.4	NOT	1999-K12
1999 HV ₁₁	1999 Apr 18.21595	13 34 59.92	-07 29 49.4	23.1	NOT	1999-K12
1999 HW ₁₁	1999 Apr 18.21595	13 35 38.83	-07 43 05.7	23.3	NOT	1999-K12
1999 HX ₁₁	1999 Apr 17.13881	12 09 31.63	+00 51 49.1	22.4	NOT	1999-K15
1999 HY ₁₁	1999 Apr 17.14936	12 32 04.84	-00 13 21.6	23.9	NOT	1999-K15
1999 HZ ₁₁	1999 Apr 17.15990	12 39 51.90	-00 28 24.3	24.0	NOT	1999-K15
1999 HA ₁₂	1999 Apr 17.19181	13 30 41.27	-05 34 46.3	23.4	NOT	1999-K15
1999 HB ₁₂	1999 Apr 18.16414	12 40 36.80	+01 25 25.3	21.9	NOT	1999-K15
1999 HC ₁₂	1999 Apr 18.34230	14 35 56.44	-10 10 06.7	22.4	NOT	1999-K15
1999 HD ₁₂	1999 Apr 17.15461	12 31 54.80	-01 03 07.9	22.9	NOT	1999-K18
1999 HG ₁₂	1999 Apr 18.20550	13 29 03.82	-09 12 07.2	23.9	NOT	1999-N11
1999 HH ₁₂	1999 Apr 18.21072	13 32 06.14	-10 43 43.0	23.9	NOT	1999-N11
1999 HJ ₁₂	1999 Apr 18.34230	14 36 05.79	-10 25 14.5	23.6	NOT	1999-N11
2000 CL ₁₀₄	2000 Feb 5.38927	10 12 09.92	+11 20 55.1	22.0	Steward	2000-E64
2000 CM ₁₀₄	2000 Feb 5.38927	10 12 32.59	+11 06 54.5	23.0	WIYN	2000-E65
2000 CN ₁₀₄	2000 Feb 5.38927	10 12 46.14	+11 12 32.0	22.5	Steward	2000-E64
2000 CO ₁₀₄	2000 Feb 6.32413	09 58 09.33	+13 57 00.2	22.8	WIYN	2000-E64
2000 CP ₁₀₄	2000 Feb 6.34632	10 09 49.80	+14 37 26.4	22.6	WIYN	2000-E64
2000 CQ ₁₀₄	2000 Feb 6.34632	10 10 34.02	+14 36 19.4	23.0	WIYN	2000-E64
2000 CE ₁₀₅	2000 Feb 5.11756	07 15 11.28	+22 36 25.9	23.0	WIYN	2000-F02
2000 CF ₁₀₅	2000 Feb 5.14503	08 11 10.84	+20 31 16.2	22.8	Steward	2000-F02
2000 CG ₁₀₅	2000 Feb 5.17626	09 04 46.05	+16 54 11.3	22.6	WIYN	2000-F02
2000 CH ₁₀₅	2000 Feb 5.41596	10 52 10.01	+06 44 39.4	22.0	Steward	2000-F02
2000 CJ ₁₀₅	2000 Feb 5.42049	10 56 37.95	+08 25 52.0	21.9	Steward	2000-F02
2000 CK ₁₀₅	2000 Feb 6.27972	08 58 53.00	+19 20 30.7	22.7	WIYN	2000-F02
2000 CL ₁₀₅	2000 Feb 6.29299	09 09 12.91	+17 58 09.0	22.4	WIYN	2000-F02
2000 CM ₁₀₅	2000 Feb 6.29758	09 13 38.01	+20 05 07.7	22.1	Steward	2000-F02
2000 CN ₁₀₅	2000 Feb 6.34632	10 10 10.23	+14 31 46.6	21.4	WIYN	2000-F02
2000 CO ₁₀₅	2000 Feb 5.13617	08 10 26.24	+22 38 16.6	22.4	WIYN	2000-F07
2000 CP ₁₀₅	2000 Feb 5.17626	09 03 44.12	+16 54 48.7	22.6	WIYN	2000-F07
2000 CQ ₁₀₅	2000 Feb 5.18506	09 15 15.36	+17 53 09.7	21.9	Steward	2000-F07
2000 CR ₁₀₅	2000 Feb 6.30637	09 14 02.39	+19 05 58.7	22.5	WIYN	2000-F07
2000 CS ₁₀₅	2000 Feb 6.38156	10 54 52.71	+10 25 07.4	22.5	Steward	2000-F07
2000 CY ₁₀₅	2000 Feb 5.16269	08 43 10.47	+17 24 14.9	23.5	WIYN	2000-F46
2000 CM ₁₁₄	2000 Feb 5.17189	08 58 49.877	+17 07 41.77	22.8	WIYN	2000-J45
2000 CN ₁₁₄	2000 Feb 5.33597	09 23 24.575	+16 40 57.29	22.2	WIYN	2000-J45
2000 CO ₁₁₄	2000 Feb 5.38049	10 01 49.008	+16 44 29.78	23.5	WIYN	2000-J45
2000 CP ₁₁₄	2000 Feb 6.27528	09 01 08.129	+20 09 49.37	23.4	WIYN	2000-J45
2000 CQ ₁₁₄	2000 Feb 6.35957	10 34 36.232	+11 36 10.00	22.6	WIYN	2000-J45
MB 4867	2000 Feb 6.30197	09 13 45.519	+19 51 16.57	23.8		

TABLE 2—*Continued*

Designation (1)	Discovery (2)	R.A. (3)	Decl. (4)	App. Mag. (5)	Recovery Telescope (6)	MPC No. (7)
MB 5355	2000 Feb 6.34632	10 08 37.952	+14 07 16.76	22.2		
MB 5487	2000 Feb 6.35957	10 33 14.801	+11 38 17.02	23.0		
MB 5560	2000 Feb 6.36836	10 48 51.282	+12 20 22.46	23.7		
1803970E	1999 Apr 18.33183	14 32 40.92	−12 06 57.9	23.8		
18040407	1999 Apr 18.33708	14 34 28.25	−12 55 53.1	24.1		
18044608	1999 Apr 18.36418	14 37 34.63	−11 08 08.3	24.4		

NOTE.—Units of right ascension are hours, minutes, and seconds, and units of declination are degrees, arcminutes, and arcseconds.

runs, one was recovered with the Perkins Telescope, eight were recovered at the 90 inch (2.3 m) Bok Telescope on Kitt Peak, and seven have not yet been recovered, because of lack of telescope time to secure the follow-up exposures in a timely manner. We are as convinced of the reality of these seven as yet unrecovered objects as we are of those bearing MPC designations, but because of the passage of time, they are now likely lost.

5.2. Orbit Determination

In predicting the positions of KBOs discovered in our survey for purposes of recovery, we calculated preliminary orbits using the method of Väisälä (1939). In this technique, it is assumed that the motion of the object is entirely tangential (i.e., the object is at perihelion or aphelion), and by further assuming the geocentric distance of the object, one can attempt to compute an orbit. At some assumed distances an orbit will be found; at others no orbit is possible. In practice, a series of candidate Väisälä orbits was computed over a range in geocentric distance from 0.1–150 AU for each slow-moving object discovered. Any object for which a potential main-belt orbit was found was removed from further analysis and review. Aphelic orbits likewise were discarded. Of those that remained, all objects had possible candidate orbits over two, and sometimes three, distinct ranges of geocentric distance. The first range was always interior to the main belt and those orbits had very small inclinations. This family represents a class of “Earth-chasing” objects moving in such a way that their orbital motion nearly matches the motion of Earth. The second range was in the “proper” range for prograde Centaurs and KBOs. This family usually covered the full range of eccentricities. The third group had retrograde orbits with very large semi-major axes. The first and third groups of candidate orbits were considered to be extremely unlikely compared with the second group comprising “normal” KBO/Centaur orbits and were discarded.

The candidate KBO-like and Centaur-like orbits in the second group spanned a large range in orbital parameter space. Ordinarily, we did not have sufficient observational coverage to permit a statistical selection from among the possibilities (e.g., by minimizing residuals). Instead, we adopted the step-by-step approach described below.

If the candidate orbits indicated a possibility of an orbit in or near the 3:2 mean motion resonance with Neptune at $a = 39.4$ AU, we searched for the existence of an allowed orbit in the resonance in which the object would avoid Neptune by at least 13 AU over the past 15,000 yr. If such an orbit was found, it was selected as the best initial provisional

orbit for the object and the object was tentatively designated as resonant.

Selection of provisional orbits for the nonresonant objects was necessarily more arbitrary. For the nonresonant KBOs, investigators, including those at the MPC, have often assumed an eccentricity near zero. However, when one projects the future position of an object with an uncertain orbit, the circular-orbit solution always places the object at the edge of the cloud representing the full range of possible future positions. We were concerned that this procedure would introduce a bias against successful recovery of objects actually in orbits of higher eccentricity. Accordingly, we have selected instead the orbit that predicts a future position in the middle of the possibilities. Typically, our approach yields an orbit with eccentricity between 0.2 and 0.4. In our judgment, this strategy works equally well for all types of objects (classical KBOs, Centaurs, and scattered-disk objects) and minimizes recovery biases.

Experience showed that this approach was effective in maximizing the likelihood of recovery. In no case was the object being sought outside the $6'7 \times 6'7$ field of view of the NFIM camera on WIYN within a 2–3 month period following discovery, even when the prediction was based on only a 2 hr arc. The WIYN frames were transmitted to Lowell Observatory and the moving objects located just as with the Mosaic data. Positions also were calculated in the usual way. In the case of objects recovered by other investigators, those individuals sometimes identified the moving objects and determined their positions independently. In either instance, the resulting coordinates were promptly transmitted to the Minor Planet Center.

Once positions of an object were available from two nights, we calculated a new Väisälä orbit using the first and last observations. In this instance, however, the residuals in the fit of the orbit to the other observations provided some guidance in selecting the preferred orbit. In cases where an object was observed during three successive lunations, the minimum in the rms residuals was ordinarily well determined and the choice of the preferred Väisälä orbit was clear-cut.

In an effort to understand the uncertainties in the orbital elements determined by this technique, we conducted a relatively extensive simulation. In this simulation, orbital elements for hypothetical KBOs were randomly chosen to approximately match the range and distribution of values displayed by known Kuiper belt objects. Then, for a particular date and observing site, we determined whether a given hypothetical object was visible within our usual observing window constraints. If so, the positions of the object at two

times on that date separated by an interval between 1.5 and 2.25 hr were computed and converted to “observed” positions by adding random noise to the positions with standard deviation of $0''.25$. This process was repeated until pairs of observations for 400 hypothetical objects were in hand. Väisälä orbits based on the pseudo-observations were then computed for each object using the same recipe as described earlier except that special attention was not given to potentially resonant orbits. The orbital elements and computed heliocentric distance at the time of discovery resulting from the analysis of the simulated data were then compared with the corresponding values for the actual orbits. This process was repeated for three additional pseudo-data sets: one including a pair of “observations” on the discovery night plus a pair 30 days later, one including pairs from the discovery night, 30 days later, and 60 days from discovery, and one including the first three pairs plus an additional pair of data points taken 1 year from the discovery night. In the last of these cases, we allowed aphelic orbit solutions in instances where they yielded smaller residuals. Because a significant number of the hypothetical KBOs were in fact near aphelion, failure to do so would have resulted in a large increase in the “errors” for the 1 year case compared with the 60 day case.

The results of the simulation are illustrated in Figure 5. In the top row, the absolute value of the “error” in the heliocentric distance of the object at the time of discovery resulting from our analysis of the pseudo data is plotted as a function of the true heliocentric distance for each of the four cases studied. On the next row is a similar display of the “error” in the inclination plotted as a function of the actual inclination and the following two rows give similar information for semimajor axis and eccentricity, respectively.

For our purposes, three important results are apparent in this figure: (1) The heliocentric distance of a KBO is determined to within a few AU even on the basis of only a pair of observations on a single night. If an object is observed during three successive lunations, that error is ordinarily no more than 2 AU. (2) The error in the inclination of an object is rapidly reduced as the object is observed in successive lunations becoming less than 2° for almost all objects with two months of coverage and less than 1° once an object is recovered in the second apparition. (3) The semimajor axis and eccentricity of KBOs are often poorly determined even after recovery in a second apparition.

While we used the Väisälä approach to predict the positions of our objects for recovery, a more sophisticated method of calculating orbits from short observational arcs recently has been published by Bernstein & Khushalani (2000). Figure 6 shows the results of the same simulation illustrated in Figure 5, except this time the Bernstein & Khushalani method was used instead of Väisälä's. It is immediately apparent that the Bernstein & Khushalani method yields a significantly better determination of r and i , and is also superior to the Väisälä approach in estimating a and e .

The trends indicated by our simulations are confirmed by an analysis of the existing database for actual KBOs. In particular, we have taken all available positional measurements from the MPC database for the 61 KBOs for which at least a 2 year span of observational data was available as of 2000 December 22. We then used the method of Bernstein & Khushalani (2000) to compute an orbit for each object using initially the data from the discovery night. Then new orbits

were computed each time observations from an additional night were available up to 90 days from the discovery. The orbital parameters (i , a , and e) resulting from each orbit solution were then compared with those from the most current orbit given for the object in the data file maintained by E. Bowell at Lowell Observatory (Bowell, Muinonen, & Wasserman 1994³) based on the full data set covering two apparitions. The differences between the orbital elements computed with the Bernstein & Khushalani (2000) method and those listed in the Bowell database are plotted as a function of time since discovery in Figure 7. Once again, we see the accuracy of the inclination determination improves rapidly over the interval plotted, while the semimajor axis and eccentricity improve more slowly.

Having explored the uncertainty in heliocentric distances and orbital elements determined from observations within a single apparition, we next ask how well the Bernstein technique predicts the location of an object in the apparition following discovery. Figure 8 shows the error in the predicted location of an object 1 year after discovery for the three simulated cases we studied (2 hr arc, 30 day arc, and 60 day arc). Note that when based on observations from a single night, the Bernstein & Khushalani (2000) approach, not surprisingly, does a comparatively poor job in predicting the object's location 1 year later. But with observations in three successive lunations, this technique predicts the future position of almost all KBOs to within one Mosaic field ($\pm 18'$).

Even in instances when one has observations from only one night, recovery of the object in the next apparition is far from hopeless for slow-moving distant objects like KBOs. In Figure 9, we have forced a large number of hypothetical KBOs having the distribution of orbital parameters used in our earlier simulations to all fall within $30''$ of a particular point in the sky (*cross*) at a particular time. This task was accomplished by selecting KBO-like orbits, as in our earlier simulations, and adjusting the mean anomaly of individual orbits at will. Objects with orbits that could not be adjusted in this way to pass within $30''$ of the point were discarded. Also plotted in the figure are the locations of these objects 1 year later and a box the size of a Mosaic frame. It is seen in the figure that most of the KBOs after 1 year of motion are clustered in a relatively tight band. Consequently, even with a totally naive approach that makes no effort to estimate a particular object's orbit, one has high probability of recovering the object with two or three Mosaic exposures.

6. RESULTS

6.1. *The Objects Discovered*

The 69 Kuiper belt objects and Centaurs discovered in this search are listed in Table 2. The objects' designations are listed in column (1) in the following order: the one KBO from our survey that has received a permanent number (19521),⁴ followed by objects with provisional MPC designations (in the order those designations were assigned), followed by the seven objects that have not yet received MPC designations. In the case of this latter group, the designations listed are our initial in-house designations. The year,

³ Available at <ftp://ftp.lowell.edu/pub/elgb/astorb.html>.

⁴ Although 19521 was discovered late in 1998, it has already received a permanent designation primarily because of prediscovery observations reported recently by Larsen et al. (2001).

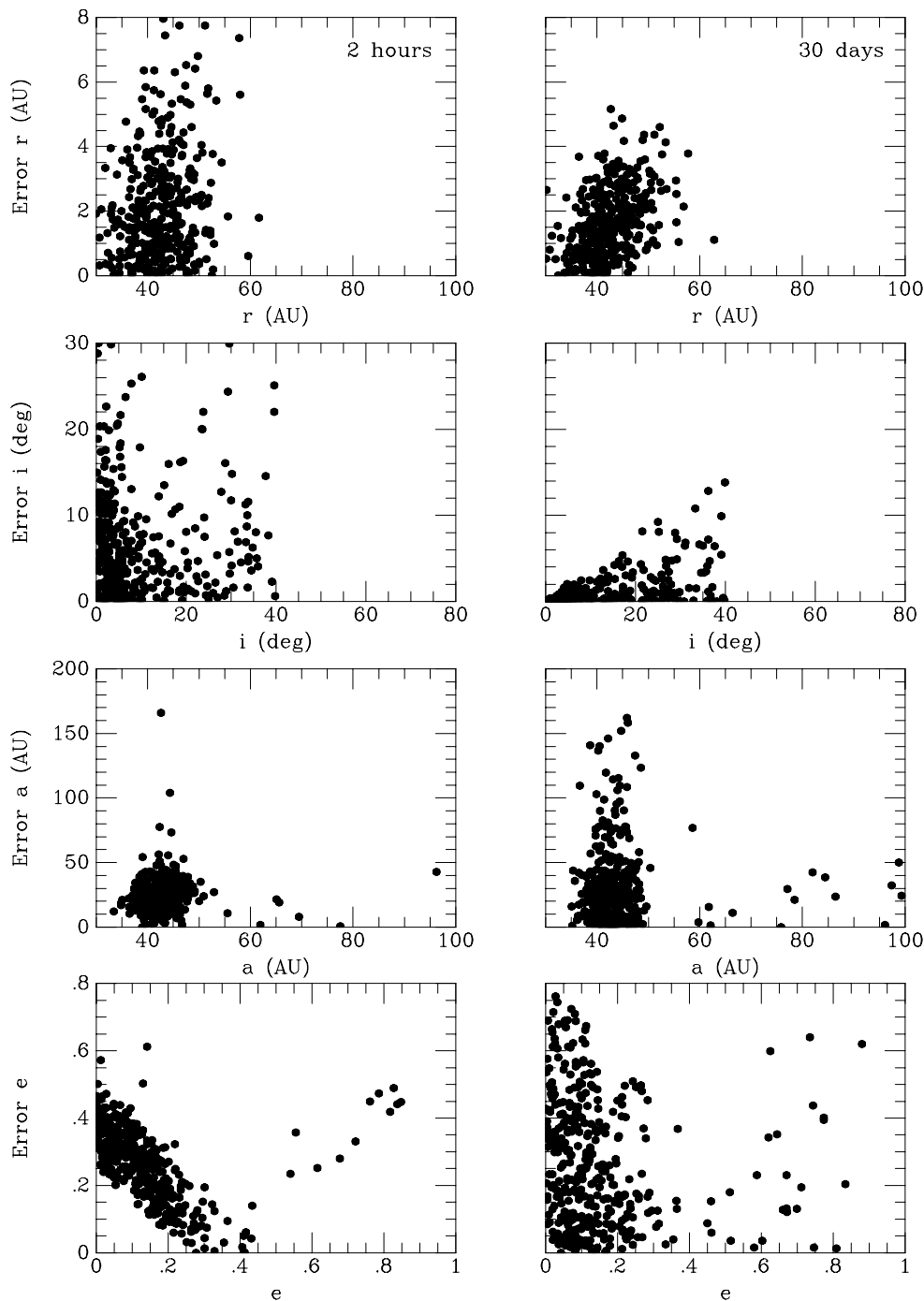


FIG. 5.—“Errors” in the calculated heliocentric distance, inclination, semimajor axis, and eccentricity of hypothetical KBO orbits as determined by the method of Väisälä (1939) for observational coverage spanning 2 hr, 30 days, 60 days, and 1 yr.

month, and day of the discovery observation and the right ascension and declination of the object at the time of discovery are listed next. The apparent magnitude is given in the next column. As discussed earlier, these numbers are uncertain by a few tenths of a magnitude except in the case of 19521, for which an accurate R magnitude was measured at the Perkins Telescope. No useful estimate of the brightness of 1998 UU₄₃ was possible from our data because of blending with a nearby stellar image. The value listed in the table is based on subsequent observations by others corrected to the date and time of discovery. The telescopes used for the recovery observations are listed in the next to last column,

followed by the identification of the Minor Planet Electronic Circular (MPEC) in which the discovery of each object that has received a designation was announced.

6.2. Orbital Elements and Uncertainties

Table 3 contains additional information for the objects discussed in this paper including their orbital elements. For each object we have listed three sets of elements of epoch 2000 February 26. Each set is based on all available observations from the MPC database as of 2001 January 20.

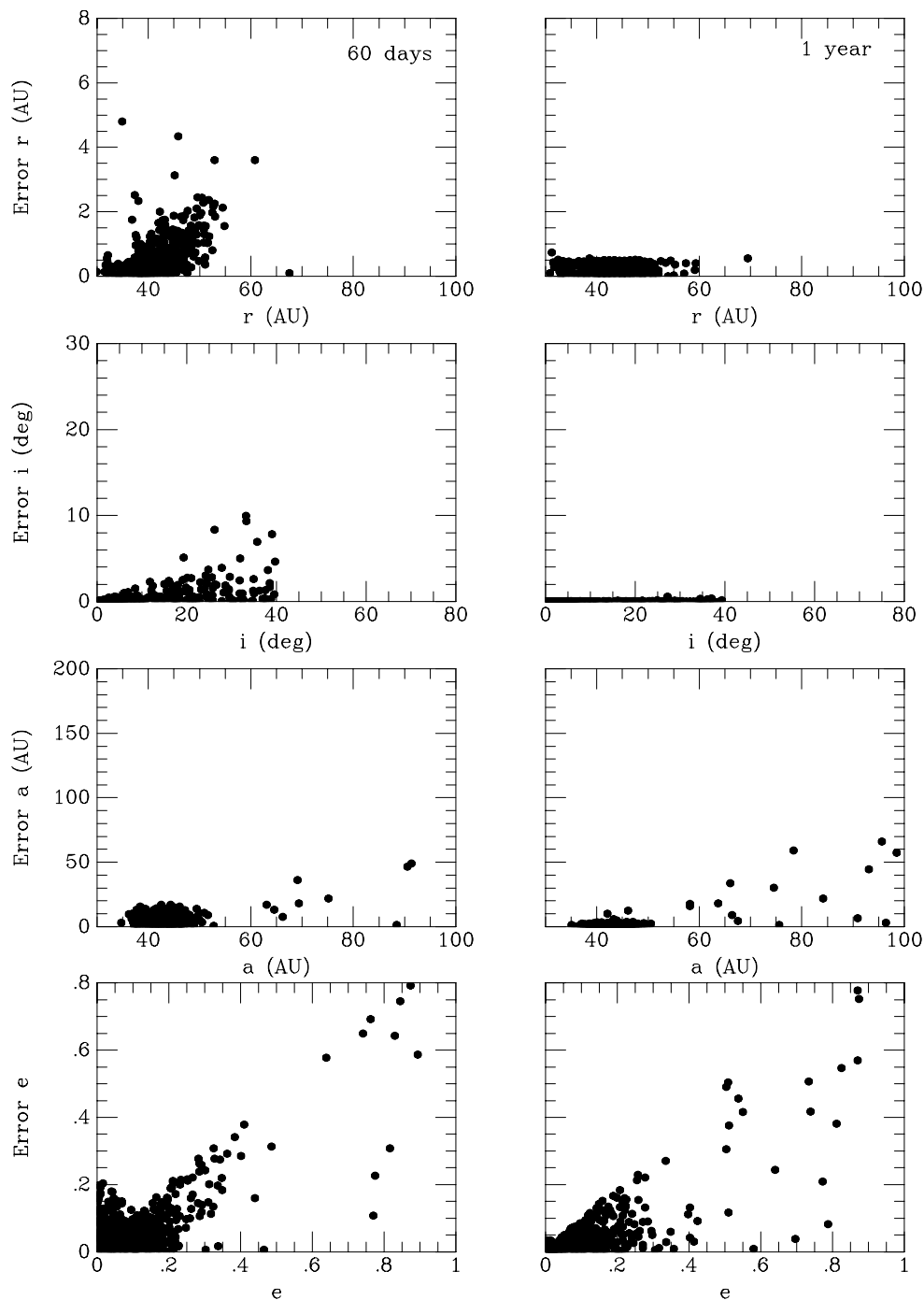


FIG. 5.—Continued

The elements listed and their associated uncertainties have been computed by different individuals using different procedures. The first line for a particular object gives elements we have computed with the method of Bernstein & Khushalani (2000), but modified to give heliocentric elements and errors rather than the barycentric values produced by the algorithm provided by those authors. The second line lists the elements by Bowell et al. (1994),⁵ and

the third line contains the elements posted on the Minor Planet Center Web site on that date. The Bowell and the MPC elements are also heliocentric. The MPC Web site does not quote uncertainties, and the Bowell site does so for only some of the objects. Whenever orbital information was required to calculate other parameters listed in Table 3, we have used the orbit based on the Bernstein & Khushalani (2000) method.

The first column of Table 3 identifies the objects in the same order and style as in Table 2. Absolute magnitudes are listed in the second column of the table. These values are based on the relevant data given in Tables 2 and 3. Next, we

⁵ As posted at <ftp://ftp.lowell.edu/pub/elbg/astorb.html> as of 2001 January 20.

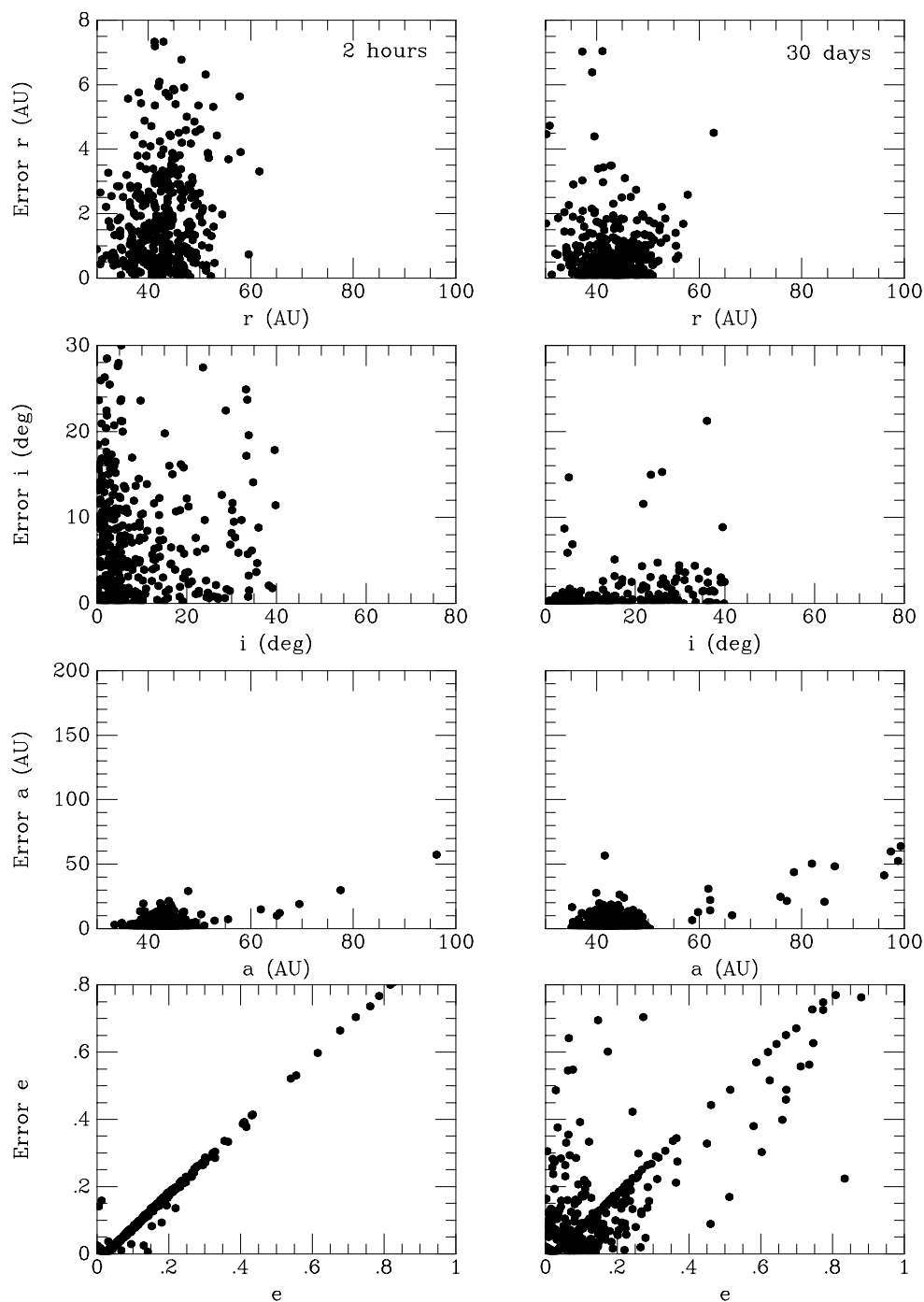


FIG. 6.—“Errors” in the calculated heliocentric distance, inclination, semimajor axis, and eccentricity of hypothetical KBO orbits as determined by the method of Bernstein & Khushalani (2000) for observational coverage spanning 2 hr, 30 days, 60 days, and 1 yr.

have indicated the total number of observations of each object in the MPC database (available by subscription) as of 2001 January 20 and the length of the interval spanned by those observations in days. Our assessment of the dynamical type of the objects is listed in column (5). If no entry appears in this column, the object’s orbit is still too uncertain to permit determination of a type. The rms residuals of the astrometric data with respect to the Bernstein & Khushalani (2000) orbit is listed in column (6). Columns (7) and (8) contain the calculated heliocentric distance of the object at the time of discovery and its perihelion distance along

with the calculated uncertainties in these parameters. The next six columns give the orbital elements and their 1σ uncertainties when available.

An examination of Table 3 quickly reveals that in the cases of objects with observational arcs sampling two or more apparitions, the orbital parameters listed by the Minor Planet Center and by Bowell usually agree well with each other and with the values we have calculated. There are, however, exceptions, such as 1999 HW₁₁ and 1999 HC₁₂, for which the MPC orbits differs substantially from those of this paper and from Bowell’s. In cases where the arc length is

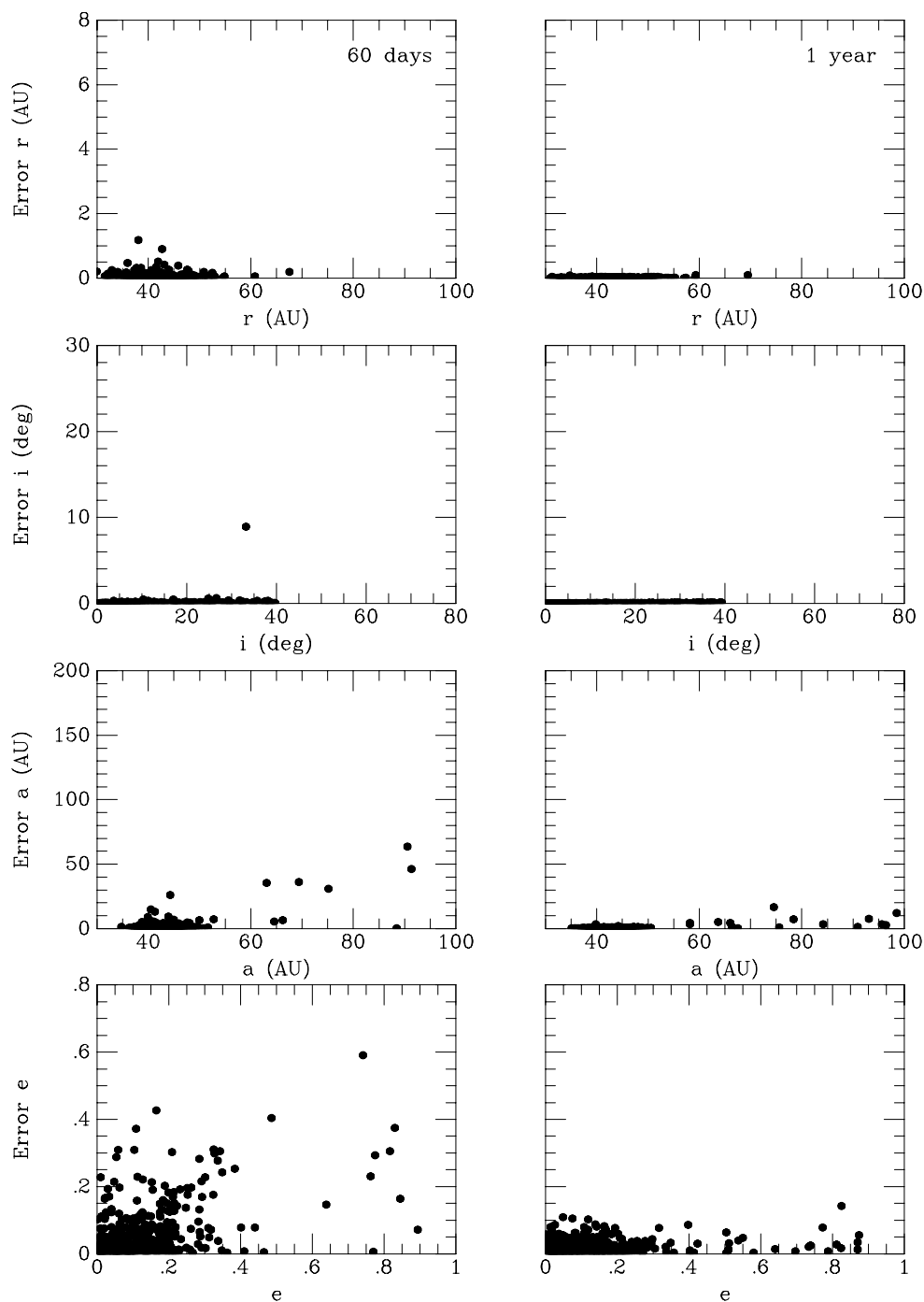


FIG. 6.—Continued

only a few tens of days, a greater dispersion in orbital elements among the three different sources is apparent and the quoted estimates of the uncertainties in these elements become similarly discrepant.

We have shown the three sets of independently calculated orbital elements for a number of reasons. First, many investigators, including the authors of this paper, in speaking and writing about Kuiper belt objects have sometimes failed to appreciate fully the uncertainties in the short-arc orbits available for most KBOs. Too often, the values available from the Minor Planet Center or at the Lowell Observatory Web site have been taken at face value and invested with a

degree of certainty far greater than the creators of those databases likely intended. Secondly, we chose to calculate our own orbits by the Bernstein & Khushalani (2000) method because that method allows calculation of uncertainties for all orbital elements in a uniform fashion regardless of arc length. In drawing general conclusions about the Kuiper belt from our sample of newly discovered KBOs, we feel that consideration of the uncertainties is essential. We have adopted the Bernstein & Khushalani (2000) error bars in the subsequent discussion portions of this paper and we have plotted them in Figures 10–12. Such error bars have been absent from many previously published papers in this

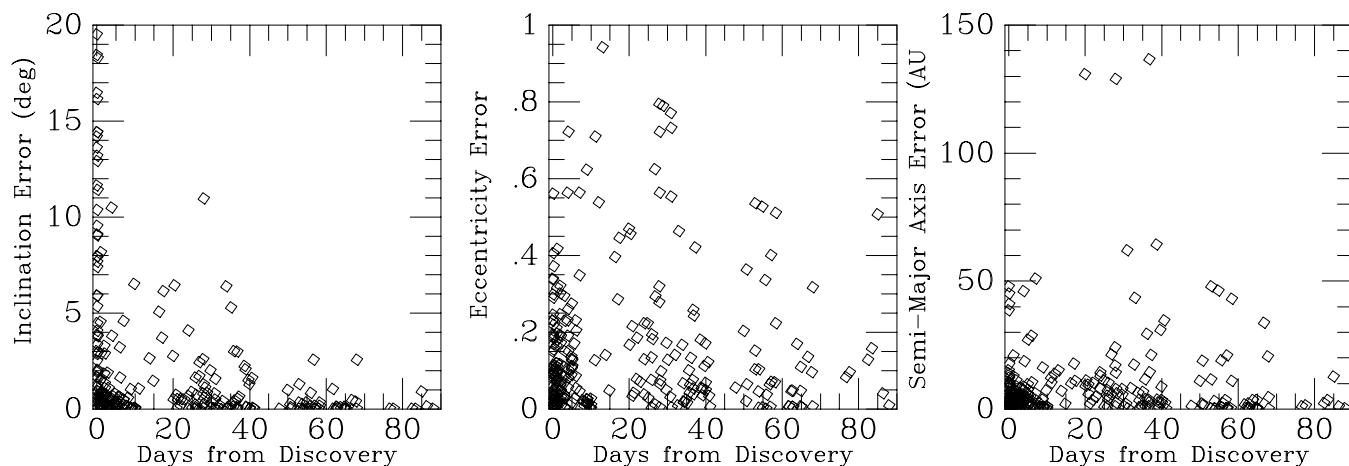


FIG. 7.—“Errors” in the orbital elements (i , a , and e) as a function of time from discovery of all KBOs known as of 2000 December 22 with astrometric observations extending over at least 2 yr. Individual points represent the difference between orbits determined by the method of Bernstein & Khushalani (2000) and the orbits from Bowell based on all available data.

field, again conveying an impression of certainty in the results that may not have been valid. Finally, we were attracted to the Bernstein & Khushalani (2000) formalism because the orbits could be calculated in a straightforward way that would be transparent to and, in principle, repeatable by the reader. The Väisälä approach and the other methods often require assumptions and choices in order to permit calculation and selection of an orbit. Those assumptions and choices, we suspect, have inadvertently shaped our current perceptions of the Kuiper belt in ways that may not be correct.

6.3. The 3:2 Mean Motion Resonance

Figure 10 shows the positions of the objects discovered in this survey as of 2000 February 26, projected onto the ecliptic plane. Triangles indicate objects we discovered in 1998, squares are objects from 1999, and diamonds are KBOs found in 2000 February. Error bars indicate the uncertainty in the heliocentric distance at the time of discovery as discussed above and listed in Table 3. When no error bar is shown, the uncertainty in heliocentric distance is smaller

than the plotted point. The orbits of the giant planets and Pluto are shown and the positions of these bodies (again on 2000 February 26) are plotted as filled circles. Also plotted (*small filled circles*) are the positions of the other 225 KBOs with designations discovered through the end of 2000 February. No error estimates have been attempted for these objects. The relative paucity of objects at ecliptic longitudes near 100° and 280° is due to the intersection of the ecliptic plane with the Milky Way. In these regions, the sky is too crowded with stars for efficient KBO searching.

Even a casual inspection of Figure 10 reveals the fraction of objects discovered near the orbit of Neptune was substantially larger in our 1998 runs than was the case in the 1999 and 2000 runs. All other things being equal, the closer objects are easier to find than the more distant ones because they are on average brighter. Consequently, some explanation for this characteristic of Figure 10 is needed.

We know that objects found near Neptune’s orbit are likely to be in a mean motion resonance with that planet. Otherwise, they would be quickly removed by gravitational interaction with the giant planet (see, e.g., Yu & Tremaine 1999). KBOs in this type of resonance are protected from

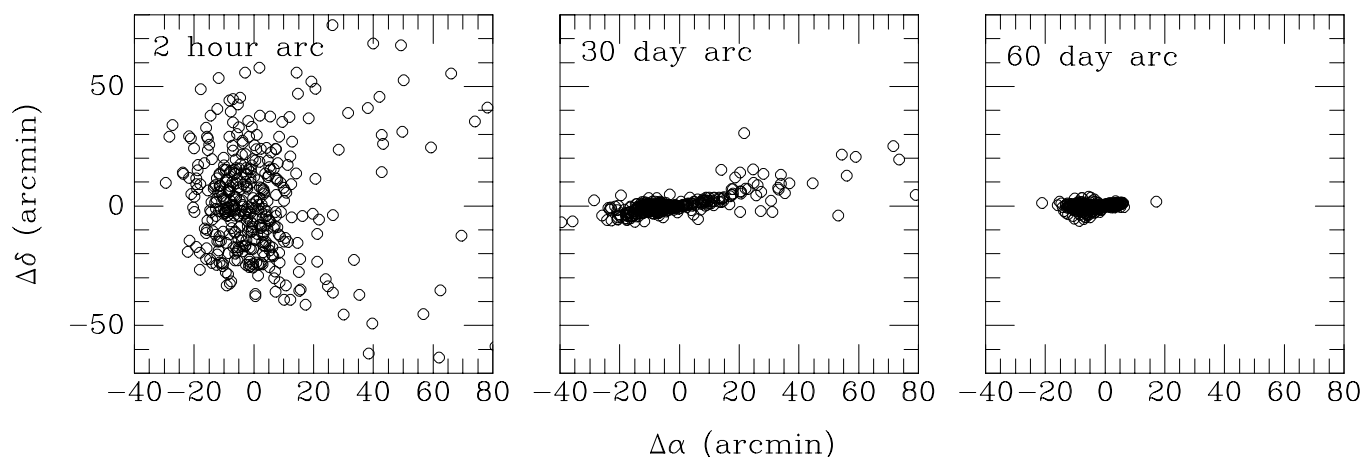


FIG. 8.—“Errors” in the predicted positions 1 year from the date of discovery of hypothetical KBOs with 2 hr, 30 day, and 60 day astrometric coverage. Predictions are based on orbits determined by the method of Bernstein & Khushalani (2000).

TABLE 3
COMPARISON OF ORBITAL ELEMENT CALCULATIONS

Designation (1)	<i>H</i> (mag) (2)	Obs. (3)	Arc (days) (4)	Type (5)	rms (6)	Discovery Heliocentric Distance (7)	Perihelion <i>q</i> (AU) (8)	Semimajor axis <i>a</i> (AU) (9)	Eccentricity <i>e</i> (10)	Inclination <i>i</i> (deg) (11)	Ascending Node <i>n</i> (deg) (12)	Argument of Perihelion <i>p</i> (AU) (13)	Mean Anomaly <i>m</i> (deg) (14)
19521	4.9	89	3360.7	CL	0.42	43.02 ± 0.00	40.93 ± 0.00 41.13 ± 0.01 41.08	45.75 ± 0.00 46.13 ± 0.01 46.16	0.105 ± 0.000 0.108 ± 0.000 0.110	12.04 ± 0.00 12.00 ± 0.00 12.00	49.98 ± 0.00 49.95 ± 0.00 49.96	57.94 ± 0.02 53.97 ± 0.04 54.67	319.28 ± 0.02 322.89 ± 0.03 322.41
1998 UR ₄₃	8.1	23	439.8	3:2	0.33	31.91 ± 0.00	30.86 ± 0.06 30.84 ± 0.08 30.81	39.79 ± 0.03 39.87 ± 0.04 39.83	0.224 ± 0.001 0.227 ± 0.002 0.227	8.74 ± 0.00 8.74 ± 0.00 8.74	53.92 ± 0.00 53.93 ± 0.00 53.93	17.23 ± 0.46 17.49 ± 0.68 18.02	339.94 ± 0.26 339.76 ± 0.35 339.41
1998 US ₄₃	7.9	12	352.2	3:2	0.26	35.23 ± 0.01	33.86 ± 0.86 33.54 ± 0.87 33.96	39.66 ± 0.29 39.94 ± 0.32 39.70	0.146 ± 0.021 0.160 ± 0.021 0.145	10.58 ± 0.00 10.57 ± 0.00 10.58	223.83 ± 0.00 223.82 ± 0.00 223.82	139.00 ± 6.95 135.79 ± 5.55 140.44	36.86 ± 4.47 38.34 ± 2.83 35.78
1998 UU ₄₃	7.2	15	763	4:3?	0.48	37.76 ± 0.00	32.21 ± 0.04 32.20 ± 0.09 32.12	36.66 ± 0.01 36.72 ± 0.02 36.70	0.121 ± 0.001 0.123 ± 0.003 0.125	9.56 ± 0.00 9.54 ± 0.00 9.54	231.33 ± 0.00 231.35 ± 0.00 231.35	276.90 ± 0.15 276.01 ± 0.34 276.29	264.61 ± 0.17 265.65 ± 0.63 265.56
1998 WG ₂₄	6.8	24	740	CL	0.19	41.32 ± 0.00	39.92 ± 0.03 39.92 ± 0.02 39.89	45.73 ± 0.01 45.92 ± 0.01 46.00	0.127 ± 0.001 0.131 ± 0.000 0.133	2.23 ± 0.00 2.22 ± 0.00 2.22	88.34 ± 0.00 88.35 ± 0.00 88.35	33.15 ± 0.24 32.48 ± 0.18 32.72	325.59 ± 0.17 326.31 ± 0.12 326.27
1998 WV ₂₄	7.3	12	736.3	3:2?	0.18	38.22 ± 0.00	37.71 ± 0.09 37.80 ± 0.07 37.82	39.20 ± 0.02 39.25 ± 0.01 39.22	0.038 ± 0.002 0.037 ± 0.002 0.036	1.51 ± 0.00 1.51 ± 0.00 1.51	183.51 ± 0.03 183.47 ± 0.02 183.48	169.74 ± 2.37 174.18 ± 2.09 174.40	49.25 ± 2.08 45.07 ± 1.84 44.96
1998 WW ₂₄	8	14	357.3	3:2	0.23	31.26 ± 0.01	29.97 ± 0.31 30.11 ± 0.29 30.03	40.31 ± 0.16 40.27 ± 0.15 40.33	0.256 ± 0.007 0.252 ± 0.007 0.255	13.91 ± 0.00 13.90 ± 0.00 13.90	233.97 ± 0.00 233.97 ± 0.00 233.98	138.04 ± 1.94 139.89 ± 1.95 138.85	23.79 ± 0.98 22.72 ± 0.89 23.21
1998 WX ₂₄	6.6	19	741.9	CL	0.34	45.12 ± 0.00	41.97 ± 0.02 42.02 ± 0.12 42.16	43.55 ± 0.02 43.61 ± 0.02 43.64	0.036 ± 0.000 0.036 ± 0.003 0.034	0.92 ± 0.00 0.92 ± 0.00 0.92	60.80 ± 0.01 60.79 ± 0.01 60.78	179.97 ± 7.62 155.32 ± 11.20 174.27	174.09 ± 7.62 200.49 ± 12.10 180.16
1998 WY ₂₄	7	21	798.8	CL	0.16	41.86 ± 0.00	41.57 ± 0.04 41.56 ± 0.02 41.53	43.34 ± 0.01 43.51 ± 0.00 43.56	0.041 ± 0.001 0.045 ± 0.001 0.047	1.91 ± 0.00 1.91 ± 0.00 1.91	102.60 ± 0.01 102.62 ± 0.01 102.62	7.49 ± 2.04 6.98 ± 1.07 7.94	329.67 ± 1.85 330.32 ± 0.96 329.53
1998 WZ ₂₄	8.1	6	64.9	...	0.13	32.90 ± 0.24	32.88 ± 3.94 30.45 ± 192.35 32.39	34.71 ± 1.82 40.13 ± 150.03 39.48	0.053 ± 0.102 0.241 ± 3.864 0.180	4.90 ± 0.19 4.57 ± 6.91 4.51	79.99 ± 0.14 80.26 ± 5.83 80.30	5.31 ± 679.99 43.45 ± 66.32 355.97	354.15 ± 610.37 332.38 ± 217.04 1.85
1998 WA ₂₅	7.2	11	735.2	CL	0.16	42.02 ± 0.01	41.03 ± 0.74 41.24 ± 0.31 41.21	42.94 ± 0.16 43.00 ± 0.06 43.00	0.045 ± 0.017 0.041 ± 0.007 0.042	1.05 ± 0.00 1.05 ± 0.00 1.05	136.35 ± 0.07 136.30 ± 0.05 136.31	209.65 ± 7.97 214.89 ± 4.46 213.95	60.75 ± 6.26 56.09 ± 3.60 56.91
1998 WA ₃₁	7	8	29.8	...	0.44	37.78 ± 0.73	37.78 ± 11.55 39.55 32.95	58.56 ± 12.08 39.76 40.15	0.355 ± 0.146 0.005 0.179	8.74 ± 0.50 10.25 10.38	19.30 ± 1.07 22.04 22.25	16.12 ± 106.38 13.73 112.3	2.00 ± 47.29 3.59 285.43
1998 WS ₃₁	8.2	18	413.1	3:2	0.32	31.50 ± 0.00	31.48 ± 0.03 31.48 ± 0.04 31.47	39.72 ± 0.02 39.78 ± 0.03 39.74	0.208 ± 0.001 0.209 ± 0.001 0.208	6.72 ± 0.00 6.73 ± 0.00 6.73	15.90 ± 0.00 15.92 ± 0.00 15.95	27.70 ± 1.39 27.90 ± 2.00 28.67	358.54 ± 0.89 358.33 ± 1.28 357.81
1998 WT ₃₁	7	13	765.2	CL	0.13	38.90 ± 0.00	37.63 ± 0.04 37.60 ± 0.02 37.56	46.32 ± 0.02 46.44 ± 0.01 46.42	0.188 ± 0.001 0.190 ± 0.000 0.191	28.61 ± 0.00 28.60 ± 0.00 28.61	41.58 ± 0.00 41.58 ± 0.00 41.58	40.49 ± 0.36 40.73 ± 0.17 41.28	335.70 ± 0.22 335.58 ± 0.11 335.22
1998 WU ₃₁	8.3	12	327.5	3:2	0.14	32.64 ± 0.01	31.68 ± 0.38 31.71 ± 0.23 31.75	39.71 ± 0.16 39.79 ± 0.10 39.75	0.202 ± 0.009 0.203 ± 0.006 0.201	6.57 ± 0.00 6.56 ± 0.00 6.56	237.16 ± 0.00 237.17 ± 0.00 237.17	138.06 ± 3.51 138.70 ± 2.14 139.13	24.68 ± 2.10 24.15 ± 1.20 23.94

TABLE 3—Continued

Designation (1)	<i>H</i> (mag) (2)	Obs. (3)	Arc (days) (4)	Type (5)	rms (6)	Discovery Heliocentric Distance (7)	Perihelion <i>q</i> (AU) (8)	Semimajor axis <i>a</i> (AU) (9)	Eccentricity <i>e</i> (10)	Inclination <i>i</i> (deg) (11)	Ascending Node <i>n</i> (deg) (12)	Argument of Perihelion <i>p</i> (AU) (13)	Mean Anomaly <i>m</i> (deg) (14)
1998 WV ₃₁	7.7	14	357.3	3:2	0.19	32.92 ± 0.01	28.83 ± 0.49	39.48 ± 0.26	0.270 ± 0.011	5.71 ± 0.00	58.57 ± 0.00	275.57 ± 1.06	41.72 ± 0.19
							28.88 ± 0.39	39.51 ± 0.21	0.269 ± 0.009	5.71 ± 0.00	58.58 ± 0.00	275.91 ± 0.85	41.48 ± 0.17
							28.91	39.42	0.266	5.71	58.57	275.92	41.70
1998 WW ₃₁ ...	6.8	8	57	CL	0.27	46.45 ± 0.03	44.77 ± 5.61	45.62 ± 0.25	0.019 ± 0.123	6.63 ± 0.03	237.19 ± 0.02	7.35 ± 1821.35	169.49 ± 1821.19
							39.95	47.34	0.156	6.57	237.22	267.54	287.47
							46.36	46.36	0.000	6.55	237.24	175.79	1.37
1998 WX ₃₁	6.6	16	741.9	CL	0.4	40.67 ± 0.00	40.60 ± 0.02	45.67 ± 0.01	0.111 ± 0.000	2.97 ± 0.00	37.41 ± 0.01	41.27 ± 0.51	352.95 ± 0.40
							40.59 ± 0.03	45.84 ± 0.02	0.115 ± 0.001	2.97 ± 0.00	37.42 ± 0.01	41.84 ± 0.97	352.52 ± 0.76
							40.58	45.88	0.116	2.97	37.46	42.61	351.89
1998 WY ₃₁	7.3	10	798.8	CL	0.11	45.30 ± 0.00	40.16 ± 0.16	45.33 ± 0.04	0.114 ± 0.004	1.97 ± 0.00	63.63 ± 0.01	105.99 ± 0.16	278.43 ± 0.46
							40.25 ± 0.07	45.51 ± 0.02	0.115 ± 0.001	1.97 ± 0.00	63.64 ± 0.00	104.19 ± 0.05	280.28 ± 0.21
							40.23	45.58	0.117	1.98	63.65	103.62	281.06
1998 WZ ₃₁	8.2	22	411.8	3:2	0.43	33.02 ± 0.00	32.89 ± 0.03	39.77 ± 0.01	0.173 ± 0.001	14.58 ± 0.00	50.54 ± 0.00	352.63 ± 1.12	11.35 ± 0.77
							32.91 ± 0.05	39.87 ± 0.02	0.175 ± 0.001	14.57 ± 0.00	50.54 ± 0.00	353.82 ± 1.81	10.47 ± 1.24
							32.93	39.87	0.174	14.57	50.54	354.39	10.08
1999 HR ₁₁	7	9	404.2	CL	0.21	42.28 ± 0.01	42.23 ± 6.61	43.44 ± 0.03	0.028 ± 0.152	3.31 ± 0.01	83.14 ± 0.65	91.84 ± 1202.88	15.71 ± 1134.55
							42.04	43.57	0.035	3.31	83.08	142.04	328.59
							42.27	43.59	0.030	3.31	83.09	107.15	1.20
2099 1999 HS ₁₁	6.7	13	354.2	CL	0.43	43.78 ± 0.01	43.06 ± 1.31	43.78 ± 0.03	0.016 ± 0.030	2.60 ± 0.00	105.58 ± 0.06	188.75 ± 3.67	273.18 ± 1.55
							43.13 ± 2.43	43.79 ± 0.05	0.015 ± 0.056	2.60 ± 0.00	105.54 ± 0.10	188.21 ± 4.87	273.49 ± 4.20
							43.27	43.87	0.014	2.60	105.51	179.58	281.98
1999 HT ₁₁	7.5	12	351.4	CL	0.2	41.65 ± 0.02	37.79 ± 2.22	43.68 ± 0.54	0.135 ± 0.050	5.06 ± 0.00	87.79 ± 0.06	195.03 ± 5.53	298.66 ± 0.94
							38.38 ± 1.84	43.51 ± 0.39	0.118 ± 0.041	5.06 ± 0.00	87.76 ± 0.05	192.87 ± 5.98	298.82 ± 1.13
							39.70	43.50	0.087	5.05	87.94	53.71	56.32
1999 HU ₁₁	6.9	20	356.6	CL	0.16	43.85 ± 0.01	40.84 ± 2.25	43.84 ± 0.25	0.068 ± 0.051	0.36 ± 0.00	51.67 ± 0.11	246.63 ± 1.66	274.85 ± 2.41
							40.32 ± 1.53	43.91 ± 0.21	0.082 ± 0.035	0.36 ± 0.00	51.79 ± 0.07	246.07 ± 0.84	276.78 ± 4.81
							41.02	43.92	0.066	0.36	51.93	244.59	276.30
1999 HV ₁₁	7.8	15	385.3	CL	0.25	43.58 ± 0.01	40.72 ± 0.36	42.71 ± 0.03	0.047 ± 0.008	3.17 ± 0.00	161.08 ± 0.02	285.76 ± 5.49	114.35 ± 5.55
							41.32 ± 0.33	42.68 ± 0.02	0.032 ± 0.008	3.17 ± 0.00	161.05 ± 0.02	271.08 ± 3.05	131.11 ± 14.28
							40.79	42.80	0.047	3.16	161.01	289.1	110.88
1999 HW ₁₁	7	13	350.4	SD	0.2	41.42 ± 0.01	39.91 ± 1.29	51.50 ± 0.61	0.225 ± 0.023	17.26 ± 0.00	198.45 ± 0.00	330.34 ± 7.49	24.02 ± 4.17
							39.32 ± 1.22	52.03 ± 0.61	0.244 ± 0.022	17.26 ± 0.00	198.45 ± 0.00	324.98 ± 5.34	26.41 ± 2.23
							33.96	61.71	0.450	17.25	198.44	302.09	25.89
1999 HX ₁₁	6.9	12	435.8	3:2?	0.39	38.30 ± 0.01	33.36 ± 2.89	38.62 ± 0.77	0.136 ± 0.073	12.79 ± 0.02	9.98 ± 0.01	77.99 ± 2.39	80.00 ± 8.36
							37.28 ± 2.92	37.97 ± 0.09	0.018 ± 0.077	12.74 ± 0.03	10.00 ± 0.02	50.92 ± 160.74	120.92 ± 171.35
							33.10	38.91	0.149	12.77	9.99	79.86	76.60
1999 HY ₁₁	8.3	6	19.9	...	0.22	39.85 ± 2.89	39.76 ± 29.66	40.56 ± 20.51	0.020 ± 0.538	6.36 ± 2.47	35.01 ± 11.46	125.75 ± 1294.73	27.28 ± 1251.10
							39.52	41.51	0.048	6.26	35.50	125.27	25.76
							39.64	42.16	0.060	6.19	35.86	151.94	1.13
1999 HZ ₁₁	8.5	6	19.9	...	0.4	36.85 ± 2.45	36.83 ± 69.01	88.26 ± 114.12	0.583 ± 0.566	8.28 ± 1.47	165.58 ± 4.58	23.19 ± 51.58	0.68 ± 10.97
							38.77	44.83	0.135	9.79	169.49	22.30	359.73
							39.05	42.38	0.079	10.06	170.06	20.01	1.13
1999 HA ₁₂	7.7	8	49.8	CL	0.27	40.66 ± 0.04	40.65 ± 0.77	42.50 ± 0.28	0.044 ± 0.017	3.57 ± 0.01	106.73 ± 0.89	94.75 ± 799.43	2.69 ± 731.22
							32.02 ± 84.70	44.02 ± 38.24	0.273 ± 1.817	3.57 ± 0.02	105.98 ± 2.88	6.69 ± 39.71	60.61 ± 163.89
							40.57	43.14	0.060	3.56	107.10	96.02	1.10

TABLE 3—Continued

Designation (1)	H (mag) (2)	Obs. (3)	Arc (days) (4)	Type (5)	rms (6)	Discovery Heliocentric Distance (7)	Perihelion q (AU) (8)	Semimajor axis a (AU) (9)	Eccentricity e (10)	Inclination i (deg) (11)	Ascending Node n (deg) (12)	Argument of Perihelion p (AU) (13)	Mean Anomaly m (deg) (14)
1999 HB ₁₂	7.5	16	355.4	SD	0.7	35.36 ± 0.01	32.80 ± 0.66	54.52 ± 0.55	0.398 ± 0.011	13.18 ± 0.00	166.50 ± 0.01	65.04 ± 1.75	343.51 ± 0.56
							33.30 ± 1.42	53.61 ± 1.10	0.379 ± 0.023	13.18 ± 0.01	166.49 ± 0.01	61.20 ± 4.62	344.37 ± 1.16
							32.62	55.37	0.411	13.16	166.44	66.17	343.55
1999 HC ₁₂	6.8	9	404.2	CL	0.29	39.15 ± 0.01	31.93 ± 4.86	48.23 ± 3.40	0.338 ± 0.089	15.38 ± 0.00	56.99 ± 0.00	87.59 ± 3.75	41.01 ± 1.29
							31.65 ± 6.06	48.64 ± 4.38	0.349 ± 0.110	15.39 ± 0.00	56.98 ± 0.01	87.05 ± 4.28	40.34 ± 7.12
							39.18	42.68	0.082	15.38	56.99	157.65	4.73
1999 HD ₁₂	12.8	11	49.8	CN	0.36	13.01 ± 0.00	12.98 ± 1.41	15.32 ± 0.01	0.153 ± 0.092	9.58 ± 0.23	177.02 ± 0.30	1.69 ± 250.21	12.93 ± 180.62
							8.20 ± 41.48	26.87 ± 83.44	0.695 ± 1.218	10.26 ± 1.38	177.82 ± 1.53	286.19 ± 24.58	17.95 ± 85.48
							8.9	21.32	0.583	10.14	177.69	288.81	26.80
1999 HG ₁₂	7.4	9	417	CL	0.22	43.09 ± 0.00	41.58 ± 1.53	42.33 ± 0.03	0.018 ± 0.036	1.03 ± 0.00	30.52 ± 0.01	356.83 ± 1945.66	177.76 ± 1945.46
							41.69	42.41	0.017	1.03	30.53	334.96	200.36
							40.13	42.55	0.057	1.03	30.54	68.12	100.18
1999 HH ₁₂	7.3	11	437.8	CL	0.29	44.09 ± 0.00	42.51 ± 0.64	43.30 ± 0.03	0.018 ± 0.015	1.30 ± 0.01	255.77 ± 0.47	130.83 ± 1900.19	179.83 ± 1900.45
							42.51	43.30	0.018	1.30	255.66	138.87	171.53
							42.70	43.39	0.016	1.31	255.58	135.54	175.08
1999 HJ ₁₂	7.3	18	434.7	CL	0.31	44.20 ± 0.00	39.54 ± 0.45	42.98 ± 0.07	0.080 ± 0.010	4.54 ± 0.00	122.54 ± 0.02	212.01 ± 3.36	254.88 ± 3.52
							39.15 ± 0.52	43.02 ± 0.09	0.090 ± 0.012	4.54 ± 0.00	122.47 ± 0.03	209.69 ± 3.03	258.38 ± 4.55
							41.37	42.79	0.033	4.54	122.47	287.74	169.84
2000 CL ₁₀₄	6.3	9	381.8	CL	0.3	42.60 ± 0.01	41.46 ± 0.39	44.26 ± 0.05	0.063 ± 0.009	1.24 ± 0.00	140.88 ± 0.02	313.21 ± 5.21	50.73 ± 4.11
							41.46 ± 0.33	44.27 ± 0.04	0.063 ± 0.007	1.24 ± 0.00	140.88 ± 0.03	313.22 ± 4.40	50.64 ± 3.41
							41.52	44.44	0.066	1.24	140.88	315.87	47.99
2000 CM ₁₀₄ ...	7.5	4	21.9	...	0.14	42.51 ± 2.53	42.49 ± 34.50	43.39 ± 23.72	0.021 ± 0.588	0.92 ± 0.35	148.99 ± 0.68	9.98 ± 1163.96	352.23 ± 1116.72
							42.35	44.44	0.047	0.90	148.96	349.19	11.52
							42.58	42.58	0.000	0.93	149.02	1.72	0.07
2000 CN ₁₀₄	7	4	24.9	...	0.1	42.83 ± 3.11	42.82 ± 34.45	43.72 ± 23.34	0.021 ± 0.589	31.04 ± 13.63	150.54 ± 0.14	6.00 ± 1164.40	354.60 ± 1117.26
							40.98	48.09	0.148	29.12	150.52	42.40	328.42
							42.93	42.93	0.000	31.52	150.54	0.26	0.07
2000 CO ₁₀₄	9.9	4	20.9	CN?	0.12	20.97 ± 2.12	20.95 ± 17.60	22.00 ± 12.04	0.047 ± 0.607	3.25 ± 1.16	351.71 ± 9.53	161.96 ± 523.07	353.55 ± 473.56
							15.38	18.59	0.173	3.74	348.24	323.79	200.10
							13.02	17.50	0.256	4.00	346.77	339.22	180.80
2000 CP ₁₀₄	7	8	63.9	CL	0.12	46.86 ± 0.05	40.15 ± 0.79	43.50 ± 0.37	0.077 ± 0.016	9.55 ± 0.06	130.74 ± 0.11	197.72 ± 446.42	180.97 ± 445.14
							40.26 ± 41.36	44.21 ± 17.43	0.089 ± 0.864	9.47 ± 1.36	130.58 ± 2.78	153.25 ± 763.48	233.07 ± 938.85
							46.46	46.46	0.000	9.17	129.94	19.26	0.06
2000 CQ ₁₀₄	8.4	8	63.9	...	0.14	35.61 ± 0.11	29.44 ± 4.75	35.64 ± 0.86	0.174 ± 0.132	13.58 ± 0.26	341.74 ± 0.26	67.28 ± 2.06	79.78 ± 11.34
							29.18 ± 19.10	35.79 ± 3.87	0.185 ± 0.526	13.58 ± 1.04	341.75 ± 1.02	67.88 ± 8.80	77.93 ± 55.12
							28.53	36.40	0.216	13.51	341.81	70.21	71.88
2000 CE ₁₀₅	7.3	9	355.1	CL	0.44	41.40 ± 0.01	41.38 ± 0.14	44.04 ± 0.04	0.061 ± 0.003	0.55 ± 0.00	76.68 ± 0.12	39.87 ± 16.19	352.55 ± 14.29
							41.18 ± 0.77	44.11 ± 0.17	0.067 ± 0.017	0.55 ± 0.00	76.67 ± 0.09	56.12 ± 29.82	338.30 ± 25.51
							41.37	44.19	0.064	0.55	76.76	40.48	351.91
2000 CF ₁₀₅	7.1	7	296.4	CL	0.21	42.26 ± 0.00	42.21 ± 6.40	43.92 ± 0.19	0.039 ± 0.146	0.53 ± 0.00	56.47 ± 0.76	49.74 ± 866.87	13.69 ± 798.81
							41.24	43.96	0.062	0.53	56.45	119.12	310.97
							41.24	44.12	0.065	0.53	56.62	117.53	312.57
2000 CG ₁₀₅	6.5	7	321.4	CL	0.09	46.45 ± 0.03	45.90 ± 0.23	46.18 ± 0.19	0.006 ± 0.003	28.02 ± 0.03	314.06 ± 0.00	0.60 ± 1161.88	179.17 ± 1161.93
							43.68 ± 2.33	46.24 ± 0.18	0.055 ± 0.050	28.03 ± 0.01	314.06 ± 0.00	277.88 ± 4.42	268.09 ± 10.22
							44.29	46.35	0.044	27.98	314.06	275.13	269.62

TABLE 3—Continued

Designation (1)	H (mag) (2)	Obs. (3)	Arc (days) (4)	Type (5)	rms (6)	Discovery Heliocentric Distance (7)	Perihelion q (AU) (8)	Semimajor axis a (AU) (9)	Eccentricity e (10)	Inclination i (deg) (11)	Ascending Node n (deg) (12)	Argument of Perihelion p (AU) (13)	Mean Anomaly m (deg) (14)
2000 CH ₁₀₅	6.8	6	64.8	...	0.23	44.28 ± 0.17	39.29 ± 3.69 40.39 ± 135.71 44.00	41.79 ± 1.26 43.11 ± 50.24 44.00	0.060 ± 0.084 0.063 ± 2.952 0.000	1.18 ± 0.03 1.15 ± 1.08 1.14	320.33 ± 0.55 319.93 ± 20.88 319.59	14.89 ± 579.61 86.43 ± 453.55 201.65	186.90 ± 578.55 108.25 ± 167.29 0.07
2000 CJ ₁₀₅	5.5	5	25	...	0.16	47.11 ± 2.76	47.04 ± 36.96 32.75 47.17	47.81 ± 25.73 40.44 47.17	0.016 ± 0.563 0.190 0.000	10.85 ± 4.17 12.57 10.96	153.66 ± 3.19 154.80 153.74	30.97 ± 1578.49 180.82 8.05	337.98 ± 1530.55 189.02 0.06
2000 CK ₁₀₅	6.4	8	364.2	...	0.14	48.47 ± 0.04	30.31 ± 0.68 29.88 ± 1.13 30.35	39.42 ± 0.46 39.62 ± 0.48 39.57	0.231 ± 0.015 0.246 ± 0.027 0.233	8.15 ± 0.01 8.16 ± 0.00 8.14	326.48 ± 0.01 326.48 ± 0.01 326.51	350.97 ± 45.17 325.94 ± 16.91 333.38	171.00 ± 44.08 210.42 ± 27.54 198.3
2000 CL ₁₀₅	6.5	8	364.2	...	0.09	45.05 ± 0.04	36.03 ± 8.43 37.87 ± 1.71 40.13	44.23 ± 2.89 43.51 ± 0.40 43.39	0.185 ± 0.183 0.130 ± 0.038 0.075	4.16 ± 0.01 4.16 ± 0.00 4.17	113.58 ± 0.04 113.59 ± 0.01 113.60	127.18 ± 14.78 133.62 ± 6.36 257.38	274.96 ± 22.48 261.54 ± 11.21 116.17
2000 CM ₁₀₅ ...	6.6	10	381	CL	0.21	41.69 ± 0.01	39.47 ± 0.39 39.48 ± 0.37 39.61	42.17 ± 0.04 42.18 ± 0.04 42.33	0.064 ± 0.009 0.064 ± 0.009 0.064	3.76 ± 0.00 3.76 ± 0.00 3.76	45.48 ± 0.03 45.48 ± 0.02 45.53	6.05 ± 1.05 6.21 ± 1.20 9.34	76.12 ± 0.16 75.94 ± 0.23 72.82
2000 CN ₁₀₅	5.6	13	376.6	...	0.16	45.72 ± 0.01	39.71 ± 1.71 40.48 ± 1.17 42.53	44.59 ± 0.41 44.39 ± 0.23 44.23	0.109 ± 0.038 0.088 ± 0.026 0.038	3.42 ± 0.00 3.42 ± 0.00 3.42	28.83 ± 0.05 28.81 ± 0.03 28.82	10.86 ± 7.45 5.66 ± 7.90 325.72	97.30 ± 8.47 105.18 ± 11.29 152.6
2000 CO ₁₀₅	5.8	12	351.3	CL	0.16	49.32 ± 0.01	40.65 ± 0.64 40.52 ± 0.18 40.87	47.00 ± 0.16 47.06 ± 0.05 47.14	0.135 ± 0.013 0.139 ± 0.004 0.133	19.27 ± 0.00 19.27 ± 0.00 19.23	307.25 ± 0.00 307.25 ± 0.00 307.26	54.06 ± 3.02 54.94 ± 0.78 55.14	104.25 ± 3.34 102.85 ± 1.28 103.26
2000 CP ₁₀₅	7.4	4	21.1	...	0.16	37.30 ± 3.10	31.67 ± 25.10 36.49 34.48	34.49 ± 16.07 40.03 83.16	0.082 ± 0.589 0.088 0.585	29.50 ± 14.28 25.95 19.43	133.27 ± 0.12 133.23 133.14	182.99 ± 278.39 3.79 1.85	177.01 ± 277.64 357.16 359.71
2000 CQ ₁₀₅	6.3	16	298.4	SD	0.2	50.97 ± 0.02	32.18 ± 4.55 32.14 ± 3.67 34.83	63.56 ± 4.89 63.74 ± 3.97 57.05	0.494 ± 0.060 0.496 ± 0.048 0.390	19.71 ± 0.01 19.71 ± 0.01 19.65	130.66 ± 0.00 130.66 ± 0.00 130.65	102.04 ± 0.60 102.00 ± 0.46 102.79	319.68 ± 2.27 319.87 ± 5.51 307.49
2000 CR ₁₀₅	6.1	10	52	SD	0.12	52.53 ± 0.07	52.53 ± 2.09 40.54 40.76	119.85 ± 3.24 792.41 675.27	0.562 ± 0.013 0.949 0.940	22.19 ± 0.12 22.86 22.85	128.08 ± 0.04 128.31 128.31	7.13 ± 53.87 309.04 309.46	0.16 ± 12.51 0.58 0.74
2000 CS ₁₀₅	7.2	4	24	...	0.04	38.80 ± 2.50	38.74 ± 30.59 38.80 38.30	39.58 ± 21.24 39.51 44.71	0.021 ± 0.567 0.018 0.143	5.24 ± 1.07 5.25 5.04	17.24 ± 8.74 17.22 19.01	164.06 ± 1193.94 149.11 141.29	340.04 ± 1140.50 354.27 0.07
2000 CY ₁₀₅	6.6	4	21.1	...	0.13	49.16 ± 2.84	49.11 ± 39.36 41.41 41.37	50.19 ± 27.33 45.59 45.53	0.022 ± 0.575 0.092 0.091	9.28 ± 3.55 10.01 10.02	133.16 ± 1.74 132.83 132.82	338.46 ± 1154.51 186.13 175.77	16.44 ± 1106.84 167.74 180.13
2000 CM ₁₁₄ ...	6.9	4	54.1	...	0.07	44.68 ± 3.10	44.65 ± 30.74 37.61 44.81	45.68 ± 20.76 41.67 44.81	0.023 ± 0.506 0.098 0.000	21.15 ± 7.75 23.02 21.5	312.33 ± 0.01 312.32 312.33	167.61 ± 1070.65 23.26 180.06	11.94 ± 1023.21 152.08 0.00
2000 CN ₁₁₄	7.3	9	53.9	...	0.19	43.58 ± 0.46	43.57 ± 6.15 43.86 44.08	48.70 ± 4.56 45.10 44.08	0.105 ± 0.094 0.027 0.000	1.54 ± 0.02 1.54 1.55	81.59 ± 0.86 82.01 82.16	54.90 ± 348.43 80.30 55.86	1.31 ± 279.99 336.99 0.00
2000 CO ₁₁₄	6.9	4	53.9	...	0.09	49.43 ± 3.86	37.80 ± 29.22 34.90 43.32	43.62 ± 18.36 43.15 46.14	0.133 ± 0.562 0.191 0.061	34.63 ± 17.81 35.55 32.51	332.71 ± 4.15 332.50 333.23	353.01 ± 165.05 24.78 352.00	179.33 ± 163.61 134.63 180.05

TABLE 3—Continued

Designation (1)	<i>H</i> (mag) (2)	Obs. (3)	Arc (days) (4)	Type (5)	rms (6)	Discovery Heliocentric Distance (7)	Perihelion <i>q</i> (AU) (8)	Semimajor axis <i>a</i> (AU) (9)	Eccentricity <i>e</i> (10)	Inclination <i>i</i> (deg) (11)	Ascending Node <i>n</i> (deg) (12)	Argument of Perihelion <i>p</i> (AU) (13)	Mean Anomaly <i>m</i> (deg) (14)
2000 CP ₁₁₄	8	4	53	...	0.14	38.86 ± 2.73	38.86 ± 29.20	47.58 ± 23.64	0.183 ± 0.460	26.44 ± 7.65	126.00 ± 2.01	5.11 ± 140.69	1.17 ± 95.42
							31.95	39.82	0.198	31.09	127.06	261.6	81.66
							32.94	39.48	0.166	31.00	127.04	260.11	86.96
2000 CQ ₁₁₄	6.6	9	378.7	...	0.18	45.09 ± 0.03	43.55 ± 4.94	45.35 ± 0.53	0.040 ± 0.108	2.70 ± 0.00	38.16 ± 0.12	33.56 ± 11.65	79.45 ± 0.61
							44.92	45.20	0.006	2.70	38.11	185.19	292.95
							43.91	45.42	0.033	2.70	38.15	197.37	283.77
MB 4867	7.7	2	0.1	...	0	44.34 ± 3.17	44.31 ± 36.10	45.33 ± 25.02	0.022 ± 0.586	8.25 ± 11.87	340.26 ± 39.63	142.77 ± 1086.37	11.19 ± 1040.35
							44.42	44.42	0.000	8.35	339.94	154.72	0.07
MB 5355	6.7	2	0.1	...	0	38.33 ± 2.83	38.32 ± 31.29	39.24 ± 21.49	0.024 ± 0.592	3.38 ± 6.50	15.01 ± 115.04	139.67 ± 1029.86	354.47 ± 974.53
							38.42	38.42	0.000	3.40	14.62	134.15	0.08
MB 5487	7	2	0.1	...	0	43.27 ± 3.18	43.24 ± 34.86	44.09 ± 24.01	0.019 ± 0.583	2.55 ± 4.71	90.76 ± 221.12	77.43 ± 1281.14	347.63 ± 1217.48
							43.34	43.34	0.000	2.56	91.15	64.08	0.07
MB 5560	8.3	2	0.1	...	0	39.43 ± 3.05	39.39 ± 31.53	40.25 ± 21.76	0.021 ± 0.578	6.18 ± 6.71	22.83 ± 61.50	153.10 ± 1177.24	343.20 ± 1123.86
							37.41	79.02	0.527	5.68	27.95	130.25	0.03
1803970E	7.5	3	0.1	...	0.23	47.09 ± 3.87	47.02 ± 37.23	47.79 ± 25.90	0.016 ± 0.568	18.09 ± 17.70	211.19 ± 8.70	30.78 ± 1593.88	339.56 ± 1546.12
							46.20	46.20	0.000	18.55	211.41	8.45	0.98
18040407.....	7.7	3	0.1	...	0.12	49.83 ± 396.36	49.82 ± 419.97	65.20 ± 546.39	0.236 ± 0.697	76.37 ± 2707	219.61 ± 105	3.05 ± 140.55	0.10 ± 73.66
							47.98	135.37	0.646	63.22	219.06	2.31	0.20
18044608.....	8.3	3	0.1	...	0.11	43.83 ± 4.16	43.78 ± 34.87	44.57 ± 23.99	0.018 ± 0.577	26.26 ± 21.29	48.29 ± 7.56	188.71 ± 1417.30	344.02 ± 1367.48
							43.97	43.97	0.000	29.15	47.35	171.86	1.06

NOTES.—For most objects three lines are given with orbital elements calculated by the following methods: (1) Bernstein & Khushalani 2000; (2) Bowell et al. 1994; (3) MPC. Only two orbits are listed for the last seven KBOs given in the table because the Minor Planet Center has not calculated orbits for these objects.

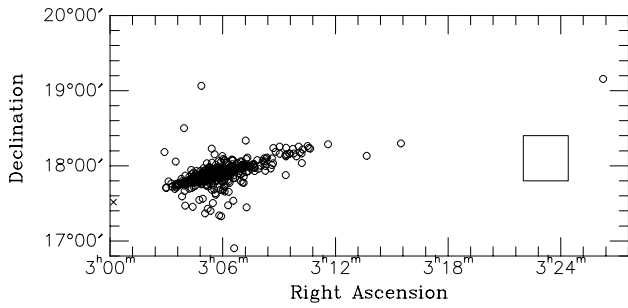


FIG. 9.—Annual motion of KBOs. The cross indicates the initial position of a population of hypothetical objects in KBO-like orbits forced by adjustment of the mean anomaly to fall within a $30'' \times 30''$ box on the sky. After 1 yr, these objects would be found at the positions indicated by open circles. The square indicates the area covered by a single Mosaic exposure.

such a fate because when they approach or cross Neptune's orbit, they do so only when Neptune is at a substantially different orbital longitude. Objects in the 3:2 mean motion resonance, which are the most numerous of the resonant KBOs, come to perihelion in longitude zones centered $\pm 90^\circ$ from Neptune and reach aphelion in zones centered on the longitude of Neptune or 180° from that point (Cohen & Hubbard 1965). In Figure 10, we see that the 2000 February observations sampled a longitude zone more or less in the opposite direction from Neptune in the sky. Consequently, KBOs in the 3:2 resonance would be expected to be near aphelion in this region, and the absence of objects near the orbit of Neptune is not surprising. The observations from 1998 and 1999, on the other hand, are located on opposite sides of the Sun-Neptune line and in the regions where the resonant KBOs come to perihelion. The substantial differ-

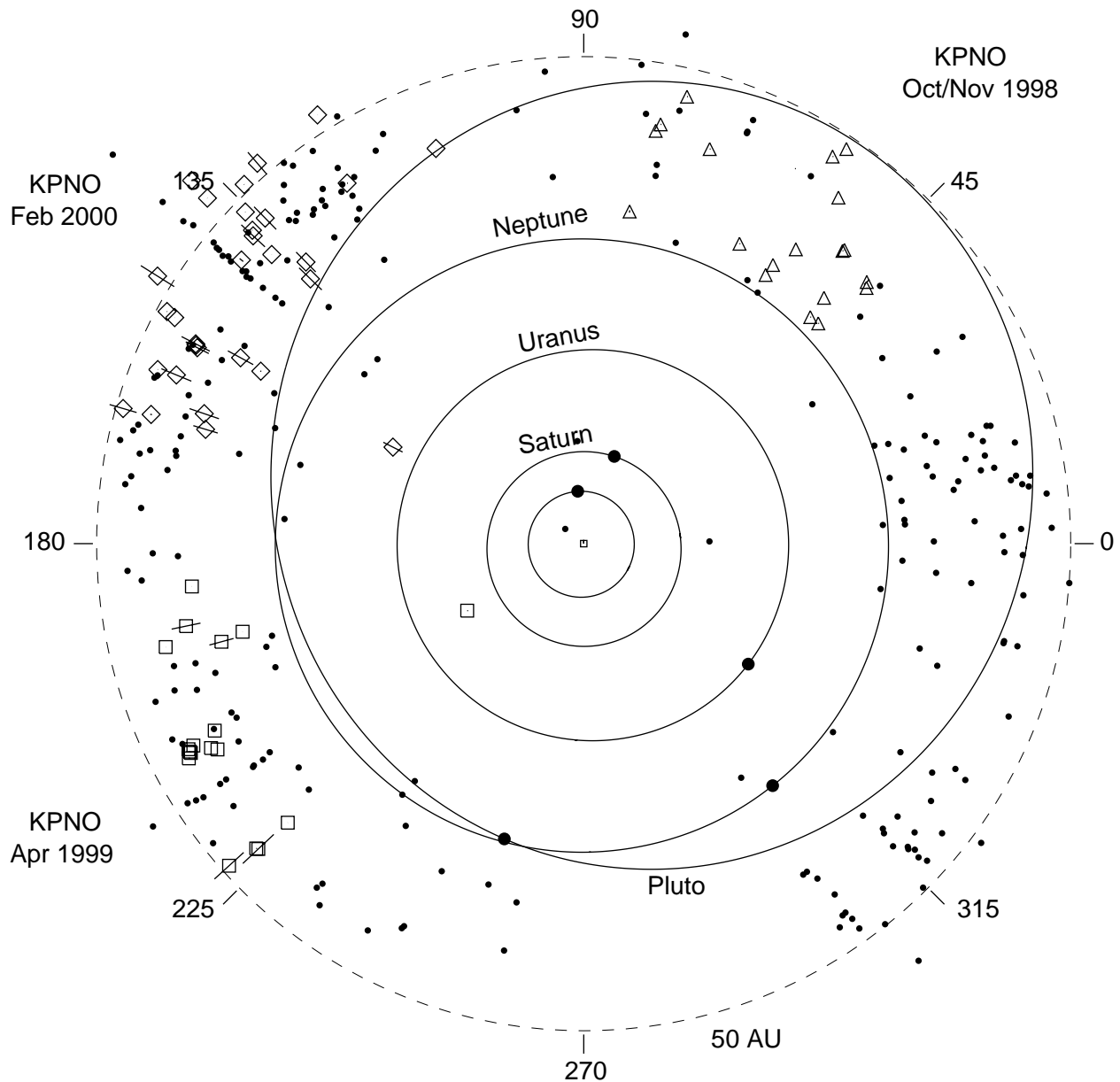


FIG. 10.—Distribution of KBOs and Centaurs discovered in this survey vs. heliocentric distance (projected onto the plane of the ecliptic) and ecliptic longitude. Triangles denote objects discovered in 1998; squares were discovered in 1999, and diamonds are objects found in 2000. Also shown are the orbits and positions of the five outer planets. The dashed circle has a radius of 50 AU. Small filled circles indicate the positions of other known KBOs.

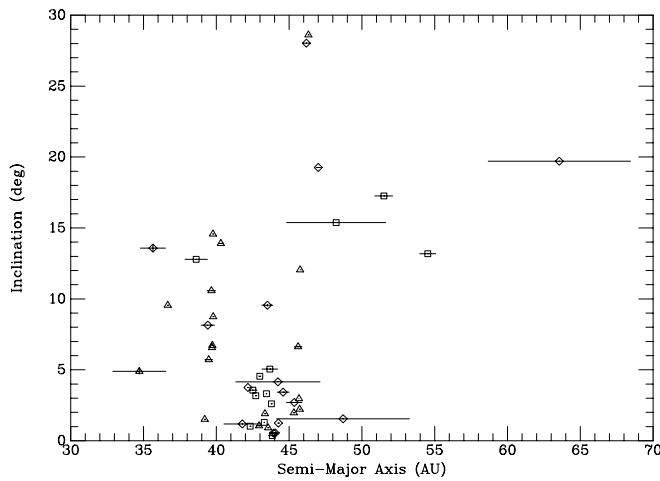


FIG. 11.—Inclination vs. semimajor axis for all objects discovered in the present investigation having uncertainties in semimajor axis less than 10 AU and which have received provisional MPC designations. Different symbols denote discoveries from different years as in Fig. 10.

ence in the relative frequency of close-in objects within these two zones therefore seems surprising. However, with our current sample sizes in the two longitude zones, the Kolmogorov-Smirnov (K-S) test (see Press et al. 1988, p. 623) indicates that the apparent difference in the distance-at-discovery distributions is not statistically significant.

The differences in the three groups of data are illustrated in another way in Figures 11 and 12. Here the inclination and eccentricity, respectively, are plotted as a function of semimajor axis for those objects in Table 3 for which the uncertainty in semimajor axis is less than 10 AU. The same symbols as in Figure 10 are used to distinguish objects from the different years. For any point not showing an error bar, the 1σ uncertainty is less than the size of the point. Note that in the 1998 data roughly half of the objects discovered were in or near the 3:2 resonance, while only one such object was found among the objects discovered in April of 1999. Here again, however, the K-S test does not establish

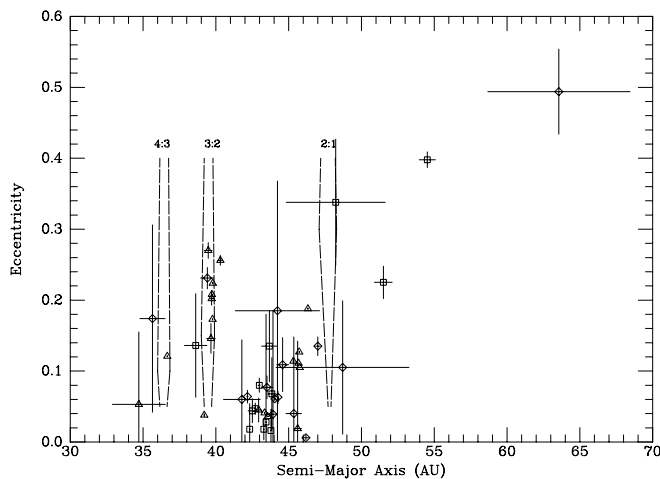


FIG. 12.—Eccentricity vs. semimajor axis for all objects discovered in the present investigation having uncertainties in semimajor axis less than 10 AU and which have received provisional MPC designations. Different symbols denote discoveries from different years as in Fig. 10. The dashed lines indicate the positions of various mean motion resonances with Neptune.

TABLE 4
KOLMOGOROV-SMIRNOV TEST

Comparison Parameters	Semimajor Axis (AU)	D^a	Significance Level
Inclination Distributions.....	$a < 41$ vs. $41 < a < 46$	0.77	2.8×10^{-5}
Eccentricity Distributions.....	$a > 46$ vs. $41 < a < 46$	0.84	1.2×10^{-4}
	$a < 41$ vs. $41 < a < 46$	0.73	6.9×10^{-5}
	$a > 46$ vs. $41 < a < 46$	0.71	1.7×10^{-3}

^a Kolmogorov-Smirnov statistic.

that the perceived difference in the two semimajor axis distributions is statistically significant. However, we will continue to watch for such an effect as our data set grows.

Another interesting characteristic of Figures 11 and 12 is that objects with semimajor axes between 41 and approximately 46 AU tend to have significantly smaller inclinations and eccentricities than KBOs found inside and outside this interval. This phenomenon has been noted before (e.g., Jewitt 1999; Jewitt & Luu 2000). However, those authors used orbital information from the Minor Planet Center, which did not include uncertainty estimates and sometimes was based on assumed values of semimajor axis or eccentricity. The point here is to show that these differences in the orbital characteristics of different classes of KBOs are statistically highly significant. We list in Table 4 the values of the K-S statistic D and the associated significance level for the comparisons mentioned above. If the inclination and eccentricity distributions were actually identical in all three semimajor axis bins, we would expect a value of D near 0.0. In fact, we find substantially larger values for this statistic. Moreover, the associated significance levels indicate that the probability of finding these high values by chance is less than 1%. We conclude that the existence of a class of “classical” KBOs in low-inclination, low-eccentricity, nonresonant orbits with semimajor axes between 41 and 46 AU is well established. Inside this zone, the resonant objects are expected to have had their inclinations and eccentricities increased by the very interactions that capture and maintain them in the resonances (e.g., Malhotra 1995). Our results are consistent with all KBOs in our data set with semimajor axes between 30 and 41 AU falling in either the 3:2 or 4:3 mean motion resonance. Beyond a semimajor axis of approximately 46 AU, we find members of the scattered disk and a couple of objects that could be in the 2:1 mean motion resonance. Here again, larger values of inclination and eccentricity are expected to be common because of the gravitational interaction of these objects with Neptune.

6.4. Other Interesting Objects

Several other dynamically interesting objects are found in Table 3. For example, 1998 UU₄₃ falls very close to the 4:3 mean motion resonance with Neptune (see Fig. 12). Based on the orbital elements listed in Table 3 for this object, we find that 1998 UU₄₃ will stay at least 11.5 AU from Neptune over the next 15,000 yr. 1998 WZ₂₄ and 2000 QY₁₀₄ may be similar objects. Both were near Neptune’s orbit when discovered, and orbits based on the Bernstein & Khushalani (2000) formalism indicate that neither object is in the 3:2

resonance. Neither do they appear to be scattered-disk objects.

Four of the objects in Table 3 have orbits characteristic of the scattered disk. 2000 CR₁₀₅ is one such object. E. Bowell and B. G. Marsden calculate orbits with semimajor axes of 700–800 AU. The Bernstein & Khushalani (2000) approach gives a much smaller semimajor axis, but even so, this object is clearly in a highly eccentric orbit that takes it far beyond the classical belt. Very recently, Gladman et al. (2001) have shown that this object has a perihelion distance no less than 44 AU. These authors discuss a number of interesting scenarios whereby an object could be placed in such an orbit. 2000 CQ₁₀₅, 1999 HB₁₂, and 1999 HW₁₁ (see Table 3) also are in orbits that take them well beyond a distance of 50 AU.

One object found in our survey, 1999 HD₁₂, is definitely a Centaur. Discovered at a distance of 13 AU from the Sun, 1999 HD₁₂, according to the Bernstein & Khushalani (2000) orbit, stays well inside Neptune’s orbit. The Bowell and MPC orbits indicate a much more elongated orbit, but the uncertainties associated with the Bowell orbit (and presumably with the MPC orbit) are very large. Another of our objects, 2000 CO₁₀₄, also is very likely a Centaur. Its heliocentric distance at discovery was 21 AU. The three independently calculated orbits for this object in Table 3 give semimajor axes in the range from 17–22 AU, but these values and the object’s eccentricity are quite uncertain.

Finally, we note that 1998 WW₃₁, discovered early in this survey, has recently been found to be a binary (Veillet 2001).

6.5. Inclination Distribution of the Kuiper Belt

In order to investigate the inclination distribution of the KBOs in our discovery sample, we removed the observational bias that arises from the fact that KBOs with significant inclinations spend more time at an ecliptic latitudes near their inclination than they do near the ecliptic equator. Since our sample is small and our intention was to compare the KBO inclination distribution with that of the short-period comets, we considered all dynamical classes as a single group. Selected for this analysis were those KBOs discovered in our survey that were observed at least four times over an interval of at least 20 days and had a formal error in the inclination determination of no more than 3°. Forty-nine of the 67 KBOs listed in Table 3 satisfy these criteria.

We then used a simple model, based on circular orbits and an assumed heliocentric reference point for the observations, to remove the observational bias for discovering more KBOs with small inclinations near the ecliptic. Denoting the ecliptic latitude by β ($-90^\circ \leq \beta \leq 90^\circ$) and the inclination of a KBO orbit by i ($0^\circ \leq i \leq 180^\circ$), we want to find the probability density function, $p(i)$, for the inclinations of the KBOs in our sample. We denote by $p(\beta, i)$ the probability density for finding a KBO of orbital inclination i when searching at an ecliptic latitude β , and we define k as a normalization constant. Then the probability density $p(\beta, i)$ is given by

$$p(\beta, i) = \begin{cases} k \frac{\cos \beta}{\sqrt{\sin^2 i - \sin^2 \beta}} p(i), & \text{if } |\sin \beta| \leq \sin i, \\ 0, & \text{if } |\sin \beta| > \sin i. \end{cases} \quad (1)$$

We used equation (1) to weight each of our search fields for

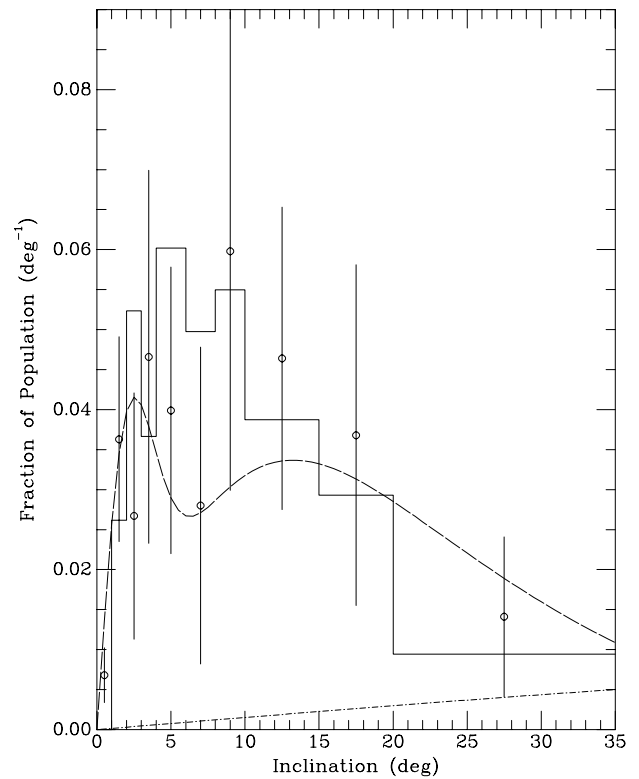


FIG. 13.—Inclination distribution for our sample of KBOs. The inclination distribution of our sample of KBOs with observational bias removed is shown by the open circles, for which the error bars have been determined from Poisson statistics. The units for the ordinate are given as the fraction of objects in the sample per degree of inclination. Our objects have been categorized into 1° bins from 0° to 4°, into 2° bins from 4° to 10°, and into 5° bins from 10° to 20° and a single bin from 20° to 35°. For reference, the inclination distribution of comets with periods less than 200 yr is shown by the solid histogram. Also for reference, we have plotted with alternating dots and dashes the $\sin i$ distribution that would be expected from a distribution of orbits with poles in random directions. The dashed curve represents the inclination distribution derived by Brown (2001).

a set of inclination intervals: 1° intervals between 0° and 4°, 2° intervals between 4° and 10°, two 5° intervals between 10° and 20°, and a single 15° interval between 20° and 35°. We then combined these weights with the number of KBOs that we discovered divided by the area searched in each of these inclination intervals to find the unbiased KBO density for each interval. Implicit in this procedure is the assumption that the inclinations of the KBOs are independent of orbital longitude and magnitude. These results are displayed in Figure 13, along with the inclination distribution of comets with periods less than 200 yr (*solid histogram*) and the $\sin i$ distribution expected for random orbits (*alternating dots and dashes*). The ordinate for these distributions is normalized to be the fraction of the population per degree of orbital inclination.

The error bars on our derived distribution for the orbital inclinations are large because of the small number of objects in the sample, but we can draw some conclusions from Figure 13. Our first conclusion is that the KBO population has an inclination distribution much more similar to that of the short-period comets than would be expected for orbits with a random distribution of inclinations. We also conclude that the lowest inclination interval (0°–1°) contains a smaller number of KBOs than its next neighbor (1°–2°). This result

agrees with the expectation that for some small interval of inclinations near zero, the inclination distribution must converge to a random distribution of inclinations [i.e., $p(i) \propto \sin i$, which increases linearly from zero at 0° inclination].

7. DISCUSSION

7.1. Comparison with Other Surveys

A number of searches for Kuiper belt objects have been conducted by others. Notable among these are the early surveys by Jewitt & Luu (1995) and Jewitt et al. (1996, 1998). The first two of these were conducted with small-format CCDs on 2 m class telescopes and covered only a few square degrees. The third survey was conducted with a detector comparable in format to Mosaic on the University of Hawaii 2.2 m telescope and reached a limiting magnitude of 22.5. A major thrust of these papers was determination and refinement of the KBO luminosity function. For reasons given earlier, we do not treat that aspect of our data in this paper. Similarly, a comparison of results such as those conveyed in Figures 11 and 12 is difficult because methods for estimating the uncertainties in the orbital elements of KBOs had not been devised at the time of these earlier papers. For example, the plot of “ e ” versus “ a ” shown by Jewitt et al. (1998), we believe, is strongly affected by the assumptions

being made at the time by the Minor Planet Center in determining KBO orbits. As a consequence, early studies tended to show a higher proportion of objects in the 3:2 resonance than we do, while objects at greater distances often were assumed to be in circular orbits.

Our survey can most meaningfully be compared with the recent survey of Trujillo, Jewitt, and Luu (Trujillo 2000; Trujillo, Jewitt, & Luu 2001) conducted primarily with an $8K \times 12K$ CCD on the 3.6 m Canada-France-Hawaii Telescope. This well-designed and carefully controlled survey covered 76 deg^2 to a limiting magnitude of 23.7 R mag and resulted in the discovery of 86 KBOs. Data were taken only on photometric nights, and the resulting magnitudes were carefully tied to Landolt standards. These authors adopted orbits determined by the Minor Planet Center or by D. Tholen. Again, no assessment of the error bars on the orbital elements was available. However, this survey yields a relative fraction of objects in the 3:2 resonance more similar to our results than did Jewitt et al. (1998), but many of the presumably classical KBOs in the study again were assumed to be in circular orbits (Trujillo et al. 2001).

Figure 14 compares the distribution of KBOs as a function of distance at the time of discovery for the Trujillo et al. (2001) survey with that found in our investigation. At first glance, one notes that while both distributions peak at the 43 AU bin, our investigation found a higher percentage of objects at larger distances and we discovered KBOs at

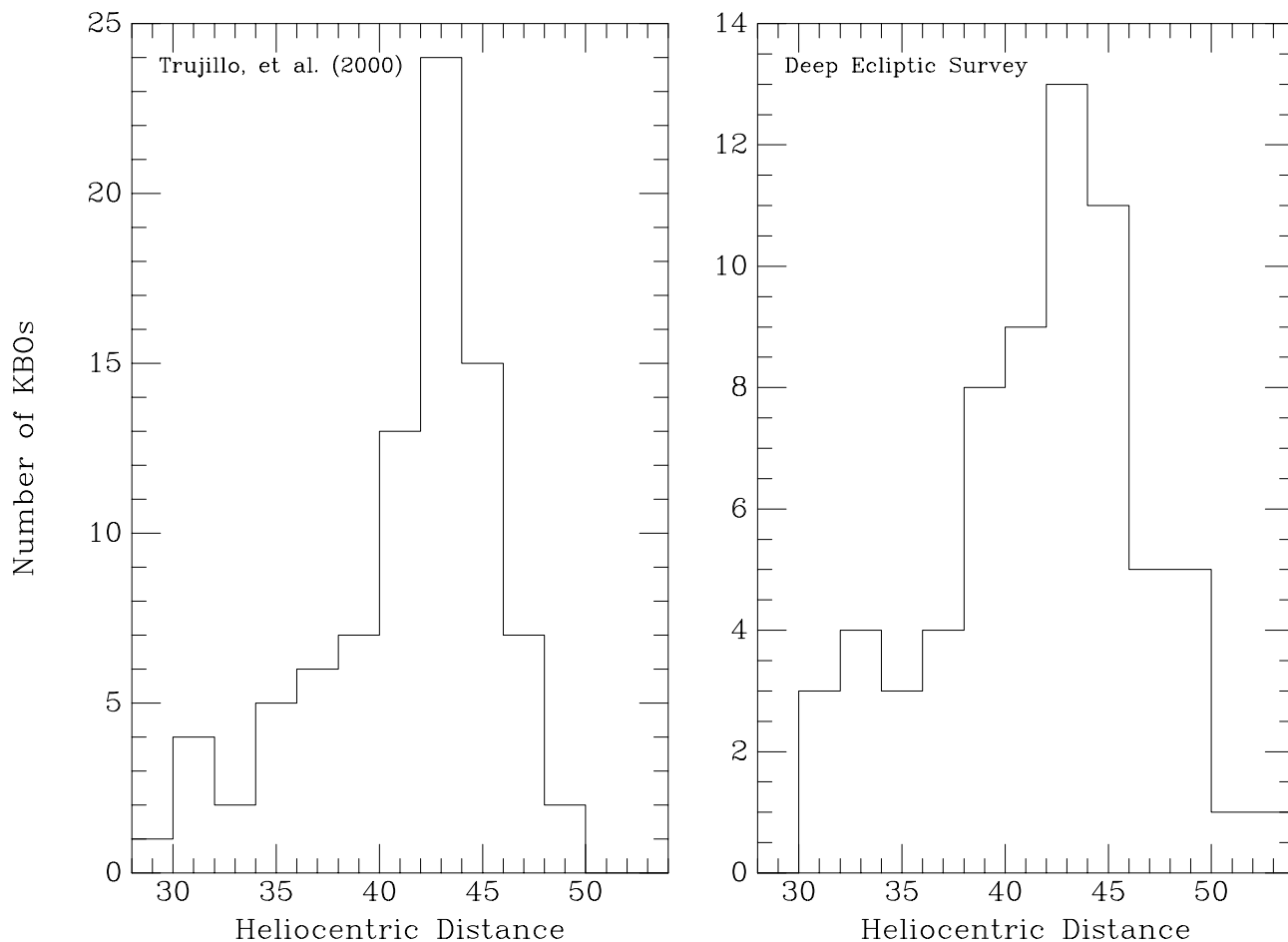


FIG. 14.—Number of KBOs as a function of heliocentric distance found in this survey and in the survey by Trujillo et al. (2001)

greater distances than did Trujillo et al. The Trujillo et al. distribution places 24 out of 87 KBOs in bins to the right of the peak, while the distribution from our survey has 23 out of 67 KBOs at these greater distances. Trujillo et al.'s two most distant KBOs were at 48.57 and 48.626 AU; ours were at 50.97 ± 0.02 and 52.53 ± 0.07 AU. While we initially thought that these facts suggested a greater sensitivity of our survey to more distant, slowly moving objects, this conclusion is not borne out by statistical tests. The Kolmogorov-Smirnov test returns a K-S statistic D of 0.089. (If the two data sets were identical, $D = 0.0$.) The probability of D being as large as 0.089 purely by chance is 92%, so we can draw no firm conclusions from the apparent differences of the two distributions in Figure 14.

It is certain that large numbers of KBOs exist at distances well beyond those that can be probed effectively with current instrumentation. Both objects found beyond 50 AU in our survey are members of the scattered disk. Objects in this category are in highly eccentric orbits, which take them in many cases to distances measured in hundreds of AU. KBOs in the scattered disk spend a small fraction of their orbital periods in the zone where we can currently detect them. Hence, the few scattered-disk objects that have been discovered require the existence of a very much greater population that cannot currently be detected. The challenge that confronts us today is to push forward as rapidly as we can with the exploration of the portion of the Kuiper belt that is accessible, while we build more appropriate instrumentation and devise better search strategies to push the frontier steadily outward.

The theoretical prediction of the Kuiper belt (Duncan et al. 1988; Fernández 1980) was based on (1) the fact that the short-period comets have only small orbital inclinations, and (2) perturbations from Neptune and subsequently the other giant planets tend not to change the orbital inclination of the perturbed body (Duncan et al. 1988). Hence, if the Kuiper belt is indeed the source of the short-period comets, we would expect the inclination distributions of these two populations to be similar. Some difference between the inclination distribution of the short-period comets and that for the total population of KBOs would be caused by the different efficiencies in the perturbation of KBOs for different dynamical classes into cometary orbits (i.e., we would expect that the resonant KBOs would be underrepresented as parents of the short-period comets and the scattered KBOs would be overrepresented). Nevertheless, the similar appearance of the two inclination distributions in Figure 13, at least to the statistical accuracy of our survey, is a striking confirmation of the theoretical prediction of the Kuiper belt.

Two other investigations of KBO inclinations—one by Trujillo (2000) and another by Brown (2001)—have used somewhat different approaches to investigate the inclination distribution. Trujillo (2000) determined the detection frequency of KBOs at ecliptic latitudes of 10° and 20° and used these measured values to determine the model parameters for Gaussian and uniform distributions of KBO inclinations with a maximum likelihood technique. Our KBO inclination distribution in Figure 13 appears to be neither a Gaussian nor a uniform distribution of inclinations, and we have not used our survey results to derive model parameters for such distributions.

Brown (2001), on the other hand, noted that one can derive the inclination distribution for KBOs by using only

those detected on the ecliptic, without the need of knowing the search fields for which no KBOs were found. He applied this method to the 143 KBOs in the MPC database on 2000 October 1 that were discovered within 0.5° of the ecliptic. His approach permits the use of a much larger sample of objects, and it differs from ours in three other ways as well. First, Brown (2001) did not remove those KBOs observed only over a few days interval, which can have large inclination errors (see Table 3) and potentially bias the results by contaminating the sample with too many high-inclination objects. Brown noted that, for objects recovered at a second opposition, “the revised inclination has differed from the initial inclination estimate by more than 3° only 4% of the time.” This is likely an underestimate of the contamination of his sample, since it does not include objects that were not recovered at later oppositions. Taken as a group, these lost objects likely have larger errors in their initial orbits than those recovered at later oppositions. We did not carry out a similar test for our objects, but we note for our designated KBOs in Table 3 that seven of 61 (11%) have formal errors in their inclination greater than 3° . Hence there is certainly a random error introduced into Brown's (2001) inclination distributions due to this sample contamination, and perhaps a systematic error as well. The systematic effect arises because the errors in the initial inclinations tend to bias them to larger values—note that most of the lines connecting the initial to final inclinations (*from diamonds to squares*) are either flat or slope downward in Brown's (2001) Figure 2.

Second, for Brown's (2001) method to be rigorously correct when he applied it to those KBO's discovered within 0.5° of the ecliptic, the search field for each discovery should have been centered on the ecliptic and have extended at least $\pm 0.5^\circ$ above and below the ecliptic. We know this was not the case for all (or perhaps any) of the KBOs used in his sample. This effect would be most pronounced on the objects with the smallest inclinations, and it may or may not be significant.

The third difference between Brown's (2001) approach (in his analysis of the entire sample of 379 objects) and ours is that he assumed that the inclination distribution function for each dynamical class (classical, Plutinos, and scattered) is well described by a dual-Gaussian distribution function, while we have made no assumptions about the shape of the distribution function. Inspection of his Figure 1*b* shows too many objects on the high-inclination (low-probability) tail of his dual-Gaussian (which may just be the effects of high-inclination contamination discussed above, or it may be indicative of a component not well described by a dual-Gaussian distribution).

In order to compare our inclination distribution with Brown's (2001) results, we have constructed an inclination distribution for the sample of KBOs used in our analysis for the Gaussian parameters given in his Table 1. This distribution is plotted as the upper dashed line in Figure 13, which agrees with our points within the error bars. A distinctive feature of Brown's (2001) distribution compared with that of the short-period comets is a dip between the two peaks at 2.5° and 13° , a hint of which appears in our distribution as well. It will be interesting to see whether this feature becomes more distinct (or disappears) in our inclination distribution as the statistics of our survey improve to the point where we can test Brown's dual-Gaussian assumption.

7.2. Plans for Future Observations

In the future, we will extend the Deep Ecliptic Survey to the full feasible range of ecliptic longitudes. Observations will be continued at Kitt Peak but also will be extended to the Blanco Telescope at Cerro Tololo Inter-American Observatory, which was recently equipped with a Mosaic camera essentially identical to the one at KPNO. Observations from CTIO will permit better coverage of those portions of the ecliptic falling at the most southerly declinations.

Increasing attention necessarily will be devoted to follow-up astrometry of previously discovered KBOs and Centaurs. As has been demonstrated in this paper, continued astrometric attention is essential to the determination of accurate orbits and such orbits are necessary not only to assure future recovery of the KBOs but also to the understanding of the dynamics of these objects. However, increasing emphasis on follow-up observations may not greatly decrease the rate at which new objects are discovered. An exposure targeted to recover an object discovered an apparition earlier is just as likely to contain a new KBO as any other spot one might choose to search.

Another goal of our continued survey will be to decrease further the time between the completion of a pair of exposures of a given field and identification of all moving objects within that field. While extreme haste in this process is not essential to the identification and recovery of KBOs, it is important to the retention of certain other classes of objects, such as NEOs, Trojans, and some Centaurs. Moreover, we have sometimes seen in our data objects moving in unexpected ways (e.g., the slowly moving prograde object in Fig. 3). Rapid detection would permit these objects to be recovered and followed rather than to become quickly lost, as is currently the case.

8. CONCLUSIONS

1. We have developed observational and analytical techniques that allow the discovery of 10–15 Kuiper belt objects and Centaurs per clear night of good seeing with the Mosaic camera on the 4 m telescope at Kitt Peak National Observatory.

2. We have demonstrated that the distance and orbital inclination of newly discovered KBOs can ordinarily be accurately determined from a few observations within a single apparition. Accurate determination of semimajor axis

and eccentricity often requires observations from two or more apparitions.

3. Essentially all KBOs with well-determined semimajor axes inside 41 AU found in our survey appear to be in either the 4:3 or 3:2 mean motion resonance with Neptune. KBOs in our sample with well determined semimajor axes between 41 and 46 AU have orbits of relatively low inclination and eccentricity, while beyond $a = 46$ AU, KBOs tend to be in orbits of relatively large orbital inclination and eccentricity.

4. Within the uncertainties imposed by our sample size, the observed inclination distribution of KBOs (averaged over all dynamical types) is similar to that of the short-period comets and is totally inconsistent with a random sample of orbital inclinations drawn from a uniform distribution.

This work benefited significantly from the able assistance of KPNO telescope operators Paul Smith, Gene McDougall, Heidi Schweiker, Kevin Edwards, Doug Williams, and particularly, Wes Cash, who often went far beyond the call of duty to support our very intense observing sessions. It was a pleasure to work with them. We also thank the KPNO director, Richard Green, and the KPNO TAC for giving us access to this outstanding telescope-instrument combination, and the KPNO mountain staff, including Jim DeVeney, Bill Schoenig, and John Glaspey, for ably and cheerfully supporting our technical and logistical requirements. Many thanks are also due to Di Harmer, Daryl Willmarth, and the other members of the WIYN Telescope staff, Matt Holman and his colleagues, and E. Fletcher and Alan Fitzsimmons for their recovery of several objects discovered in this survey. Kim Falinski and Matt Holman assisted at the 4 m during the 1999 April run. Finally, we thank the referee, Michael E. Brown, for his very helpful comments and suggestions. This work was supported in part by NASA grants NAG 5-3940, 5-4195, and 5-8990. The NOAO observing facilities used in this investigation are supported by the National Science Foundation. The Nordic Optical Telescope is operated on the island of La Palma jointly by Denmark, Finland, Iceland, Norway, and Sweden, in the Spanish Observatorio del Roque de los Muchachos of the Instituto de Astrofísica de Canarias.

REFERENCES

- Allen, R. L., Bernstein, G. M., & Malhotra, R. 2001, *ApJ*, 549, L241
 Barucci, M. A., Romon, J., Doressoundiram, A., & Tholen, D. J. 2000, *AJ*, 120, 496
 Bernstein, G., & Khusalani, B. 2000, *AJ*, 120, 3323
 Bowell, E., Muinonen, K., & Wasserman, L. H. 1994, in *IAU Symp.* 160, *Asteroids, Comets, Meteors 1993*, ed. A. Milani, M. di Martino, & A. Cellino (Dordrecht: Kluwer), 477
 Brown, M. E. 2000, *AJ*, 119, 977
 ———. 2001, *AJ*, 121, 2804
 Buie, M. W., & Bus, S. J. 1992, *Icarus*, 100, 288
 Chiang, E. I., & Brown, M. E. 1999, *AJ*, 118, 1411
 Cochran, A. L., Cochran, W. D., & Torbett, M. V. 1991, *BAAS*, 23, 1314
 Cohen, C. J., & Hubbard, E. C. 1965, *AJ*, 70, 10
 Davies, J. K., Green, S., McBride, N., Muzzerall, E., Tholen, D. J., Whiteley, R. J., Foster, M. J., & Hillier, J. K. 2000, *Icarus*, 146, 253
 Duncan, M., Quinn, T., & Tremaine, S. 1988, *ApJ*, 328, L69
 Fernández, J. A. 1980, *MNRAS*, 192, 481
 Gladman, B., Holman, M., Grav, T., Kavelaars, J., Nicholson, P., Aksnes, K., & Petit, J.-M. 2001, *Icarus*, submitted (astro-ph/0103435)
 Gladman, B., Kavelaars, J. J., Nicholson, P. D., Lored, T. J., & Burns, J. A. 1998, *AJ*, 116, 2042
 Holman, M. J., & Wisdom, J. 1993, *AJ*, 105, 1987
 Irwin, M., Tremaine, S., & Żytkow, A. N. 1995, *AJ*, 110, 3082
 Jewitt, D. 1999, *Annu. Rev. Earth Planet. Sci.*, 27, 287
 Jewitt, D., & Luu, J. 1993, *Nature*, 362, 730
 ———. 1998, *AJ*, 115, 1667
 Jewitt, D., Luu, J., & Chen, J. 1996, *AJ*, 112, 1225
 Jewitt, D., Luu, J., & Trujillo, C. 1998, *AJ*, 115, 2125
 Jewitt, D. C., & Luu, J. X. 1995, *AJ*, 109, 1867
 ———. 2000, in *Protostars and Planets IV*, ed. V. Mannings, A. P. Boss, & S. S. Russell (Tucson: Univ. Arizona Press)
 Kowal, C. T. 1989, *Icarus*, 77, 118
 Larsen, J. A., et al. 2001, *AJ*, 121, 562
 Levison, H. F., & Duncan, M. J. 1990, *AJ*, 100, 1669
 ———. 1997, *Icarus*, 127, 13
 Luu, J., & Jewitt, D. 1996, *AJ*, 112, 2310
 Luu, J. X., & Jewitt, D. 1988, *AJ*, 95, 1256
 Luu, J. X., & Jewitt, D. C. 1998, *ApJ*, 502, L91

- Majewski, S. R., Kron, R. G., Koo, D. C., & Bershady, M. A. 1994, *PASP*, 106, 1258
- Malhotra, R. 1995, *AJ*, 110, 420
- Muller, G. P., Reed, R., Armandroff, T., Boroson, T. A., & Jacoby, G. H. 1998, *Proc. SPIE*, 3355, 577
- Press, W. H., Flannery, B. P., Teukolsky, S. A., & Vetterling, W. T. 1988, *Numerical Recipes in C* (Cambridge: Cambridge Univ. Press)
- Rousselot, P., Lombard, F., & Moreels, G. 1999, *A&A*, 348, 1035
- Sheppard, S. S., Jewitt, D. C., Trujillo, C. A., Brown, M. J. I., & Ashley, M. C. B. 2000, *AJ*, 120, 2687
- Tegler, S. C., & Romanishin, W. 1997, *Icarus*, 126, 212
- Trujillo, C., & Jewitt, D. 1998, *AJ*, 115, 1680
- Trujillo, C. A. 2000, Ph.D. thesis, Univ. Hawaii
- Trujillo, C. A., Jewitt, D. C., & Luu, J. X. 2001, *AJ*, 122, 457
- Tyson, J. A., Guhathakurta, P., Bernstein, G. M., & Hut, P. 1992, *BAAS*, 24, 1127
- Väisälä, Y. 1939, *Informo Astron.-Opt. Inst. Turku Univ.*, No. 1
- Veillet, C. 2001, *IAU Circ.* 7610
- Yu, Q., & Tremaine, S. 1999, *AJ*, 118, 1873